

Parity-to-charge conversion for readout of topological Majorana qubits

Gábor Széchenyi¹ and András Pályi^{2,*}

¹*Institute of Physics, Eötvös University, H-1117 Budapest, Hungary*

²*Department of Theoretical Physics and BME-MTA Exotic Quantum Phases "Momentum" Research Group, Budapest University of Technology and Economics, H-1111 Budapest, Hungary*

(Dated: February 19, 2024)

We theoretically study a scheme to distinguish the two ground states of a one-dimensional topological superconductor, which could serve as a basis for the readout of Majorana qubits. The scheme is based on parity-to-charge conversion, i.e., the ground-state parity of the superconductor is converted to the charge occupation on a tunnel-coupled auxiliary quantum dot. We describe how certain error mechanisms degrade the quality of the parity-to-charge conversion process. We consider (i) leakage due to a strong readout tunnel pulse, (ii) incomplete charge Rabi oscillations due to slow charge noise, and (iii) charge relaxation due to phonon emission and absorption. To describe these effects, we use simple model Hamiltonians based on the ideal Kitaev chain, and draw conclusions to generic one-dimensional topological superconductors wherever possible. In general, the effects of the error mechanisms can be minimized by choosing a smooth shape and an optimal strength for the readout tunnel pulse. In a case study based on InAs heterostructure device parameters, we estimate that the parity-to-charge conversion error is mainly due to slow charge noise for weak tunnel pulses and leakage for strong tunnel pulses.

CONTENTS

I. Introduction	1
II. Parity-to-charge conversion for a two-site Kitaev chain	2
III. Error mechanisms for a two-site Kitaev chain	4
A. Leakage due to strong readout tunnel pulse	5
B. Incomplete charge Rabi oscillations due to slow charge noise	5
C. Charge relaxation due to phonon emission	6
IV. Discussion	9
A. Parity readout in a long Kitaev chain in the ideal limit	9
B. Smooth tunnel pulse leads to better readout	10
C. Refinements of the noise model	10
D. Potential extensions of the phonon analysis	11
E. Parity readout as a generalized measurement	11
V. Conclusions	12
Acknowledgments	12
A. Low-energy description of parity-to-charge conversion	12
B. Perturbative calculation for the leakage-induced parity readout error	13
1. Two-site Kitaev chain	13
2. Three-site or longer Kitaev chains	13
C. Perturbative calculation of the parity readout error due to slow charge noise	14
D. Charge relaxation due to phonon emission at finite temperature	14

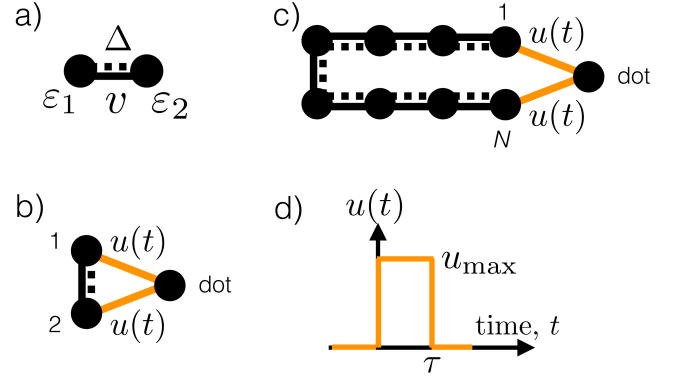


FIG. 1. Quantum-dot-assisted parity readout of a 1D topological superconductor. (a) Two-site Kitaev chain with an effective superconducting gap Δ , hopping amplitude v , and on-site energies $\varepsilon_{1,2}$. (b) Geometry of a parity readout scheme based on tunneling-induced charge Rabi oscillation between the chain (1,2) and the readout dot (dot). (c) Geometry of the same parity readout scheme with a longer Kitaev chain, $N = 8$. (d) Step-like tunnel pulse inducing the Rabi oscillation between the chain and the dot.

E. Bogoliubov-de Gennes formalism for dynamics	15
References	16

I. INTRODUCTION

One-dimensional topological superconductors (1DTSs) are thought to provide useful hardware^{1–4} for topological quantum computing.⁵ The ground state of such a superconductor is two-fold degenerate, and the two ground states are distinguished by their fermion parity, one being even and the other being odd. This degen-

eracy is robust against local perturbations, which is a key feature providing protection against certain types of decoherence. Recent experiments have been providing more and more evidence of 1DTS behavior, most notably via transport experiments combining s-wave superconductors with semiconductors,^{6–10} or spinful atomic chains.^{11–13} The natural next step is to try quantum information experiments with qubits based on the robust ground-state degeneracy of 1DTSs, often referred to as Majorana qubits.¹⁴

A key primitive toward reading out Majorana qubits is the ability to distinguish between the even and odd ground states of a single 1DTS, a procedure that is often called ‘parity readout’.^{15–17} The phrase ‘parity readout’ is also used for the measurement of the occupation of a single non-local fermionic mode shared by two Majorana zero modes.^{18–23} The significance of parity readout is especially pronounced in measurement-only topological quantum computing schemes.^{18,24} Direct parity readout is hindered by the same features that protect the Majorana qubit from decoherence. Therefore, the parity information should first be converted to a physical quantity that is easy to measure. One possibility is to convert the parity information to charge information.^{16,18} We note that in this work, the word ‘parity’ is used to describe the ground-state fermion number parity, and not the global fermion number parity, as, e.g., in Refs. 25 and 26.

Here, we describe a scheme allowing for parity readout of a single 1DTS wire (Fig. 1c), which is a preliminary version of the joint parity readout of two or four Majorana zero modes. In our scheme, parity readout is achieved via parity-to-charge conversion and a subsequent charge readout. The parity-to-charge conversion stage uses a nearby quantum dot (see Fig. 1b, c), and the parity information of the wire is converted to the occupation of the quantum dot. Clearly, the error of the parity readout is a key figure of merit for the performance of future devices based on Majorana qubits. Hence, we consider and quantitatively describe realistic mechanisms, including slow charge noise and phonon-mediated inelastic processes, which make this parity-to-charge conversion scheme imperfect. Our results provide guidelines for future experiments aiming at demonstration and optimization of the parity readout procedure.

The viewpoint we take is that quantum-information experiments with 1DTSs are expected in the near future, and therefore practical questions regarding feasible experiments will arise. For example, a relevant question is: based on the knowledge acquired in the previous decades of coherent-control experiments with solid-state qubit devices (superconducting qubits, spin qubits), what are the feasibility conditions for the upcoming topological quantum information experiments? Our work provides guidelines in that respect: see, e.g., the results summarized in Fig. 5, the map showing the proximity gap and readout pulse strength required to achieve a certain parity readout fidelity.

We note that in practice, a single 1DTS wire is not

sufficient for encoding a qubit, but at least two wires are required for that.³ Nevertheless, the minimal setup where parity-to-charge conversion could be demonstrated is the single-wire setup considered here. Extending our study to a two-wire scenario could reveal different error mechanisms, e.g., related to charge dipole formation.²¹

The rest of the paper is organized as follows. In section II, we outline our model and define the parity readout error. In section III, we calculate the parity readout error induced by three different error mechanisms: leakage due to a strong readout tunnel pulse, incomplete charge Rabi oscillations due to slow charge noise, and charge relaxation due to phonon emission. In a case study based on InAs heterostructure device parameters, we estimate that the parity readout error is mainly due to the first two error mechanisms. In section IV, we discuss generalizations of our results, and provide conclusions in section V.

II. PARITY-TO-CHARGE CONVERSION FOR A TWO-SITE KITAEV CHAIN

A simple model of a 1DTS, often termed the *Kitaev chain*, have been formulated by Kitaev.¹ Besides serving as a minimal 1DTS model, it has been proposed that the the few-site Kitaev chain can be realized by combining a few superconducting electrodes with a few quantum dots.^{27–29}

We start our analysis with the two-site Kitaev chain. Together with a third site representing a quantum dot used for charge readout (the *readout dot* or simply *dot*, see Fig. 1b), our setup is described by the Hamiltonian

$$H = H_{\text{chain}} + H_{\text{dot}} + H_{\text{tun}} \quad (1a)$$

$$H_{\text{chain}} = \varepsilon_1 c_1^\dagger c_1 + \varepsilon_2 c_2^\dagger c_2 + v(c_1^\dagger c_2 + h.c.) + \Delta(c_1^\dagger c_2^\dagger + h.c.) \quad (1b)$$

$$H_{\text{dot}} = \varepsilon_{\text{dot}} c_{\text{dot}}^\dagger c_{\text{dot}} \quad (1c)$$

$$H_{\text{tun}} = u(t)(c_1^\dagger c_{\text{dot}} + c_2^\dagger c_{\text{dot}} + h.c.) \quad (1d)$$

Here, the Hamiltonian H_{chain} of the Kitaev chain is built up from the fermion creation and annihilation operators (c), and it includes the on-site energies ε_1 and ε_2 of the chain, the normal hopping amplitude v , and the effective superconducting gap $\Delta > 0$. The Hamiltonian H_{dot} of the readout dot is parametrized by the on-site energy ε_{dot} . Finally, the chain-dot tunneling Hamiltonian H_{tun} is parametrized by the time-dependent hopping amplitude $u(t)$, which is a non-negative real quantity throughout this work. One possible generalization of our model is to take into account the spin degree of freedom.^{30,31}

For now, we consider the *ideal Kitaev limit*, where the tunneling amplitude within the chain matches the effective superconducting gap, $v = \Delta$, and the on-site energies are zero, $\varepsilon_1 = \varepsilon_2 = \varepsilon_{\text{dot}} = 0$. Later, we will describe the effect of disorder by considering the on-site energies as random variables. Following earlier work, we will consider parameter sets where the effective superconducting

gap is a few tens or hundreds of microelectronvolts,²⁸ and the on-site disorder is of the order of $1\text{ }\mu\text{eV}$.³²

To describe the parity readout mechanism, we use the complete Fock-space Hamiltonian here. However, often it is insightful and sufficient to apply a low-energy description of the coupled chain-dot system.¹⁵ We summarize that alternative low-energy picture in Appendix A.

Before specifying the parity readout procedure and defining the parity readout error, we introduce a convenient basis of the many-body states. Since Eq. (1) describes a spinless fermionic model with three sites, the dimension of the full Fock space is 8. The Hamiltonian conserves the parity of fermion numbers, hence the dynamics is governed by two separate 4×4 Hamiltonians. It is convenient to use a product basis, composed of the energy eigenstates of H_{chain} and H_{dot} . The energy eigenbasis of H_{chain} is expressed in the occupation number representation as

$$|e\rangle = \frac{1}{\sqrt{2}}(|11\rangle - |00\rangle), \quad (2)$$

$$|e'\rangle = \frac{1}{\sqrt{2}}(|11\rangle + |00\rangle), \quad (3)$$

$$|o\rangle = \frac{1}{\sqrt{2}}(|10\rangle - |01\rangle), \quad (4)$$

$$|o'\rangle = \frac{1}{\sqrt{2}}(|10\rangle + |01\rangle), \quad (5)$$

whereas the eigenbasis of H_{dot} will be denoted as $|0\rangle$ (empty dot) and $|1\rangle$ (filled dot). Note that $|e\rangle$ and $|o\rangle$ are the even and odd ground states of H_{chain} , at energy $-\Delta$, whereas $|e'\rangle$ and $|o'\rangle$ are the excited states, at energy $+\Delta$.

Using the product basis of the even sector ordered as $|e, 0\rangle, |o, 1\rangle, |e', 0\rangle, |o', 1\rangle$, the Hamiltonian matrix of this sector reads

$$H_e = \begin{pmatrix} -\Delta & u(t) & \frac{1}{2}(\varepsilon_1 + \varepsilon_2) & 0 \\ u(t) & -\Delta + \varepsilon_{\text{dot}} & u(t) & \frac{1}{2}(\varepsilon_1 - \varepsilon_2) \\ \frac{1}{2}(\varepsilon_1 + \varepsilon_2) & u(t) & \Delta & 0 \\ 0 & \frac{1}{2}(\varepsilon_1 - \varepsilon_2) & 0 & \Delta + \varepsilon_{\text{dot}} \end{pmatrix} \quad (6)$$

Using the produce basis of the odd sector ordered as $\{|o, 0\rangle, |e, 1\rangle, |o', 0\rangle, |e', 1\rangle\}$, the Hamiltonian matrix of this sector reads

$$H_o = \begin{pmatrix} -\Delta & 0 & \frac{1}{2}(\varepsilon_1 - \varepsilon_2) & 0 \\ 0 & -\Delta + \varepsilon_{\text{dot}} & -u(t) & \frac{1}{2}(\varepsilon_1 + \varepsilon_2) \\ \frac{1}{2}(\varepsilon_1 - \varepsilon_2) & -u(t) & \Delta & u(t) \\ 0 & \frac{1}{2}(\varepsilon_1 + \varepsilon_2) & u(t) & \Delta + \varepsilon_{\text{dot}} \end{pmatrix} \quad (7)$$

The eigenstates of the Hamiltonians H_e and H_o for $\varepsilon_1 = \varepsilon_2 = \varepsilon_{\text{dot}} = 0$ and $u(t) = 0$, i.e., the basis states defined above, are depicted in the energy level diagrams of Fig. 3a and b, respectively. The matrix elements of the tunneling Hamiltonian H_{tun} are also depicted, as the orange arrows connecting the energy levels.

We envision the parity readout protocol as follows. Initially, the dot is empty, and we set the dot level in resonance with the chain chemical potential: $\varepsilon_{\text{dot}} = 0$.

The charge dynamics allowing for the readout is triggered by switching on the tunneling between each end of the chain and the readout dot (Fig. 1b), using the following squared-shape tunnel pulse (Fig. 1d):

$$u(t) = u_{\text{max}}\Theta(t)\Theta(\tau - t). \quad (8)$$

Here, τ is tunnel pulse duration, and $u_{\text{max}} > 0$ is the tunnel pulse strength. We will also refer to u_{max} as the readout speed.

Using the 4×4 matrix representations of the Hamiltonians H_e and H_o , it is straightforward to see how this pulse allows for the parity-to-charge conversion. For the simple case when all on-site energies are zero, the 2×2 low-energy block (top left block) of H_e has an off-diagonal element u , whereas the same block of H_o has zero in the off-diagonal. That implies that if the system starts in the even ground state $|e, 0\rangle$, then it will Rabi-oscillate to the state $|o, 1\rangle$, but this Rabi oscillation does not happen when the initial state is $|o, 0\rangle$. After a half Rabi oscillation, the parity of the wire is therefore converted to the charge of the readout dot, which can be measured by a proximal charge sensor.³³

To evaluate the quality of the parity readout, we introduce the *parity readout error* ϵ as follows. We assume that the initial state is the one where the chain is in one of its ground states, either in the even or in the odd state, and the quantum dot is empty. The readout procedure consists of a tunneling time window and the subsequent charge measurement. Using our model, we can calculate how the probabilities of finding the quantum dot empty or filled upon charge measurement depends on the initial state, denoted as $P_{0 \leftarrow e}, P_{1 \leftarrow e}, P_{0 \leftarrow o}, P_{1 \leftarrow o}$. These probabilities fulfill the normalization conditions $P_{0 \leftarrow e} + P_{1 \leftarrow e} = 1$ and $P_{0 \leftarrow o} + P_{1 \leftarrow o} = 1$, therefore only 2 out of these 4 quantities are independent. Ideally, the charge measurement gives a clear distinction between the two different initial states, i.e., $P_{0 \leftarrow e} = P_{1 \leftarrow o} = 0$ and $P_{0 \leftarrow o} = P_{1 \leftarrow e} = 1$. The non-ideal nature of the readout procedure is therefore characterized by the *parity readout error*

$$\epsilon = \max\{P_{0 \leftarrow e}, P_{1 \leftarrow o}\}. \quad (9)$$

The concept of the parity readout error is exemplified using Fig. 2a. Focus on the time evolution shown by the dashed lines. The black (gray) dashed line shows the dot occupation probability as the function of the readout pulse duration for the even (odd) initial state, for a two-site Kitaev chain in the ideal limit. These curves reveal that $P_{1 \leftarrow o} \approx 0$ whereas $P_{1 \leftarrow e} \approx 0.75$. The latter implies $P_{0 \leftarrow e} \approx 0.25 \gg P_{1 \leftarrow o}$, hence the parity readout error defined in Eq. (9) is $\epsilon = P_{0 \leftarrow e}$. E.g., a pulse duration $\tau \approx 2\hbar/\Delta$ implies a parity readout error $\epsilon \approx 0.25$. In the rest of the paper, we will use ϵ to quantify the imperfect nature of the readout procedure.

To be more precise, the parameter ϵ characterizes *single-shot* readout error. This is the relevant figure of merit for many quantum-information protocols, including quantum error correction,³⁴ sampling algorithms,³⁵

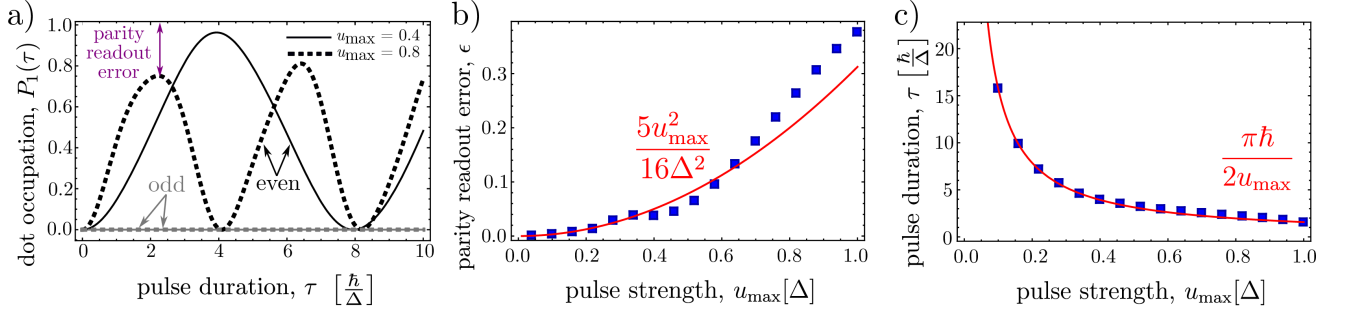


FIG. 2. Parity readout error due to leakage caused by a strong readout pulse. (a) Time evolution of the occupation probability $P_1(\tau)$ of the readout dot, for the two different initial states (even and odd), and for two different readout pulse strengths (see legend). (b) Parity readout error as a function of the readout pulse strength. (c) Numerically obtained optimized readout pulse duration (boxes) and its comparison to the analytical estimate (solid).

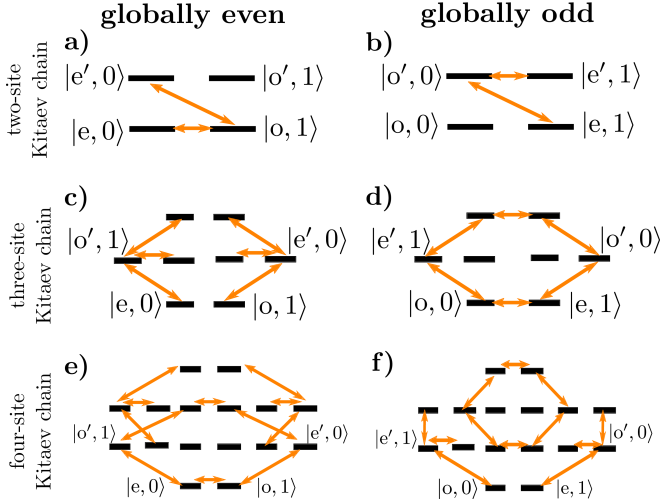


FIG. 3. Energy levels and chain-dot tunneling matrix elements in a simple model of parity readout. Horizontal lines are the energy levels of the composite system of the Kitaev chain and the readout dot, described by $H_{\text{chain}} + H_{\text{dot}}$. Orange arrows are the nonzero tunneling matrix elements of H_{tun} .

and measurement-based quantum computing, e.g., one-way quantum computing.³⁶

There are a few different proposals for the readout of Majorana qubits, and some of them were suggested to enjoy exponential protection against certain error mechanisms, e.g., the one based on continuous charge measurement of an auxiliary dot.^{18,20,37,38} The Rabi-oscillation-based scheme^{16,20} we study here requires fine tuning of pulse shape and timing, and hence does not enjoy exponential protection against, e.g., such pulse errors. Nevertheless, there are strong reasons motivating the analysis of such non-protected protocols, including the one presented in this work.

(1) *Experiments.* There are many experiments probing charge Rabi oscillations in quantum-dot systems, see, e.g., Refs. 39–41; this is a well established experimental setting in the field of quantum devices. The readout scheme studied here is a natural extension, and our re-

sults can help the design and the analysis of such a future experiment.

(2) *A strong measurement is a simple measurement.* One advantage of the Rabi-oscillation-based readout scheme studied here is its conceptual simplicity, as compared to exponentially protected schemes, e.g., based on continuous charge readout.^{18,20,37,38} Our scheme offers a straightforward way to calculate the probabilities of the measurement outcomes, even in the presence of quasiparticle excitation (aka *leakage*, see section III A), as it uses a strong, von Neumann-type measurement in a setting where the readout dot is decoupled from the Kitaev chain. On the other hand, in the exponentially protected readout scheme (e.g., continuous charge readout), the analysis must incorporate a measurement theory, that is, a detailed description of the interaction of the measurement device with the measured system, (e.g., electrons flowing in a quantum point contact whose current reveals the charge of the readout dot). Recent theory works^{37,38} make important steps in that direction, but - perhaps in part due to the complexity of the measurement model - those works do not incorporate charge noise, do not incorporate quasiparticle excitation errors (leakage), and do not provide results for the readout fidelity.

(3) *Rapid measurement.* In an experiment, when the system size and the excitation gap are both fixed and finite, decoherence mechanisms (e.g., quasiparticle poisoning) impose an upper bound on the readout time. The protocol we study here is fast, enabling readout before decoherence happens. This can be an advantage with respect to adiabatic protocols, which, in principle, enjoy exponential protection in the adiabatic limit, but decoherence might obstruct reaching that limit.

III. ERROR MECHANISMS FOR A TWO-SITE KITAEV CHAIN

In this section, we quantify the imperfect nature of the parity-to-charge conversion, using the simplest possible model for the 1DTS, the two-site Kitaev chain intro-

duced in Eq. (1). In the three subsections, we describe three mechanisms: (A) leakage, (B) incomplete charge Rabi oscillations, and (C) charge relaxation. These arise due to (A) a strong tunnelling pulse, (B) slow charge noise inducing a random on-site energy component on the readout dot, and (C) phonon-mediated inelastic processes.

Our motivation for a detailed study of the two-site Kitaev chain as a minimal model is threefold. First, this is a minimal model where the derivations can be followed easily. Second, it turns out that this minimal model exhibits and exemplifies all error mechanisms we see on longer chains, and the order-of-magnitude of errors does not depend significantly on the chain length, see Figs. 5, 7 and 8 below. Third, an analysis of the two-site Kitaev chain model is important for future experiments where a Kitaev chain is built from quantum dots.^{27–29} There, the simplest device is of course a two-site chain; it is not expected to show topological physics, but is a natural and important building block to study.

A. Leakage due to strong readout tunnel pulse

Even in the absence of noise, the tunnel pulse between the 1DTS and the readout dot induces transitions between the low-energy states and high-energy states having finite-energy quasiparticles in the chain. This *leakage* gets stronger for stronger tunnelling pulse.

First, we illustrate this leakage mechanism and its dependence on the tunnel pulse strength u_{\max} in Fig. 2a. The gray curves in Fig. 2a show the readout dot occupation after a tunneling pulse of duration τ , for the case when the chain is in its odd state initially. For both the weaker (solid) and stronger (dashed) tunnel pulse, $P_1(\tau) = 0$, which is perfect for the parity-to-charge conversion. The black curves show the readout dot occupation after a tunneling pulse of duration τ , for the case when the chain is in its even state initially. Naturally, the stronger pulse (dashed) provides a faster readout, with an optimal pulse duration of $\tau \approx 2\hbar/(0.8\Delta)$, compared to the weaker pulse (solid) with an optimal pulse duration of $\tau \approx 2\hbar/(0.4\Delta)$.

Another feature of the black curves is that there is a finite parity readout error for both tunneling pulse strengths, the stronger pulse resulting in a greater error (marked with the ‘parity readout error’ label). The reason for this error is leakage, that is, that the high-energy excited states of the system acquire a finite population during the tunnel-induced dynamics, and they get more populated if we choose a stronger tunnel pulse. This role of the excited states is illustrated in Fig. 3a, where the orange arrows depict the tunneling-induced matrix elements between the eigenstates of the uncoupled wire-dot Hamiltonian. This level diagram shows that the state $|0, 1\rangle$ is tunnel-coupled to the high-energy excited state $|e', 0\rangle$, leading to increasing leakage with increasing tunnel pulse strength.

To quantify the parity readout error due to leakage, we determine its optimum for various values of the tunnel pulse strength. We numerically simulate the time evolution of the parity-to-charge conversion process to obtain the readout dot occupation $P_{1\leftarrow e}(\tau)$, and numerically find its first maximum, providing optimal parity readout. This minimal error is shown as the discrete data set (boxes) in Fig. 2b as a function of the tunnel pulse strength u_{\max} , revealing a clear trend that a slower readout is more reliable.

A perturbative analytical treatment of the dynamics (see appendix B) valid for $u_{\max} \ll \Delta$ yields an analytical result for the parity readout error,

$$\epsilon = \frac{5}{16} \left(\frac{u_{\max}}{\Delta} \right)^2. \quad (10)$$

This function is plotted as the solid line in Fig. 2, showing a reasonable agreement with the numerical data set, especially in the slow readout range, $u_{\max} \ll \Delta$, where the perturbative treatment is justified. Note that the numerically optimized tunnel pulse durations, shown as the data set (boxes) in Fig. 2c, show hardly any deviations from the analytical expression $\tau_{\text{ideal}} = \pi\hbar/(2u_{\max})$ (solid line) derived for a two-level Rabi oscillation.

B. Incomplete charge Rabi oscillations due to slow charge noise

A generic feature of mesoscopic electronic devices is the presence of electric potential fluctuations,³² often characterized by a frequency-dependent power spectrum $S(f)$ proportional to $1/f$.^{42–44}

Due to the dominance of the low-frequency component, we will refer to this type of noise as *slow charge noise*, and, following earlier works,^{45–48} will use a quasistatic model to describe it. In our model, we account for the most prominent effect of this noise, which is to detune the energy level of the readout dot. Because of this detuning, charge Rabi oscillations are only partial, and hence the parity-to-charge conversion is imperfect. As we show (Fig. 4a), the main effect of the slow charge noise is that the parity readout error increases as the tunnel pulse strength is decreased. Given the fact that the leakage error increases with increasing tunnel pulse strength, our conclusion is that in the presence of slow charge noise, there is an *optimal* tunnel pulse strength that minimizes the parity readout error.

To reach that conclusion, we assume that the on-site energies of both the Kitaev chain and the readout dot are random. Furthermore, we model slow charge noise as quasistatic, by which we mean that its configuration is time-independent for any single run of the experiment, and changes randomly between different runs. For example, in the case of a two-site Kitaev chain, we model the three on-site energies ε_1 , ε_2 and ε_{dot} as independent random Gaussian variables with zero mean and the same standard deviation σ_{noise} .

We mimic experimental conditions by first optimizing the parity readout scheme for the tunnel pulse duration, and assuming that the system is subject to noise already during this optimization. First, we generate $N_r = 5000$ random realizations of the on-site energy vector $\xi = (\varepsilon_1, \varepsilon_2, \varepsilon_{\text{dot}})$, which we call disorder realizations from now on, and denote as ξ_j ($j \in \{1, 2, \dots, N_r\}$). Second, we simulate the coherent dynamics of the parity readout procedure, i.e., the charge Rabi oscillation, for each disorder realization, yielding the disorder-dependent occupation probabilities $P_{1 \leftarrow e}(t, \xi)$ and $P_{1 \leftarrow o}(t, \xi)$ of the readout dot. Third, we evaluate the disorder-averaged readout dot occupation probabilities, $\bar{P}_{1 \leftarrow e}(t) = (1/N_r) \sum_{j=1}^{N_r} P_{1 \leftarrow e}(t; \xi_j)$ and $\bar{P}_{1 \leftarrow o}(t) = (1/N_r) \sum_{j=1}^{N_r} P_{1 \leftarrow o}(t; \xi_j)$. Finally, we numerically find the shortest time t where the parity readout error has a local minimum as the function of t ; this we call the optimized tunnel pulse duration τ_{opt} .

The optimized tunnel pulse duration τ_{opt} is of course a function of the tunnel pulse strength u_{max} . This functional dependence $\tau_{\text{opt}}(u_{\text{max}})$ is shown in Fig. 4b as the data points (blue boxes), for the case when the noise strength is $\sigma_{\text{noise}} = 0.01\Delta$, computed from $N_r = 5000$ realizations. For comparison, we also show the function $\tau_{\text{ideal}}(u_{\text{max}}) = \frac{\pi\hbar}{2u_{\text{max}}}$, which describes the optimal tunnel pulse duration expected from idealized, complete two-level charge Rabi oscillations. We conclude that there is no observable difference between the numerically optimized τ_{opt} and analytically estimated τ_{ideal} values of the optimal tunnel pulse duration.

Next, we simulate the effect of slow charge noise on the parity readout error. Since slow charge noise is modelled as a random vector ξ of the on-site potentials, the parity readout error is also a random variable. We consider a specific value for the noise strength $\sigma_{\text{noise}} = 0.01\Delta$, fix the tunnel pulse strength u_{max} , and apply a tunnel pulse of duration $\tau_{\text{opt}}(u_{\text{max}})$. Then, the parity readout error is characterized by a probability density function $\rho(\epsilon; u_{\text{max}})$. The data points (blue boxes) in Fig. 4a show the average parity readout error as a function of the tunnel pulse strength u_{max} , as obtained from finite-sample averaging with $N_r = 5000$ disorder realizations. The error bars in Fig. 4a connect the 1st and 9th deciles of the N_r parity readout values.

The average parity readout error shows a non-monotonic behavior as u_{max} is increased. For slow readout, that is, small u_{max} , the parity readout error grows as the readout speed is reduced. For fast readout, the parity readout error grows as the readout speed is increased. The latter feature is caused by leakage, as discussed in the previous subsection. The former feature is a consequence of the disorder. More precisely, in the weakly disordered regime ($\sigma_{\text{noise}} \ll \Delta$) studied here, the only relevant component of the disorder is the random on-site energy of the readout dot. The randomness of the on-site energies of the Kitaev chain has hardly any effect on the results, since the energy detuning suffered by the chain eigenstates are second order in the disorder, as seen by

the fact that ε_1 and ε_2 does not appear in the diagonals of the matrices H_e and H_o of Eqs. (6) and (7).

In fact, the simple structure of the Hamiltonians H_e and H_o allows us to derive an analytical estimate for the parity readout error, in the limit when $\sigma_{\text{noise}} \ll u_{\text{max}} \ll \Delta$. The derivation, based on textbook perturbation theory, is outlined in appendix C. The resulting formula for the parity readout error is

$$\epsilon = \frac{5}{16} \left(\frac{u_{\text{max}}}{\Delta} \right)^2 + \frac{1}{4} \left(\frac{\sigma_{\text{noise}}}{u_{\text{max}}} \right)^2 \quad (11)$$

This analytical result is shown as the solid line in Fig. 4a, providing a reasonable approximation of the numerical data (blue boxes). Note that the perturbative calculation in appendix C reveals that the parity readout error in this two-site model is dominated by the first-order effect that the on-site energy of the readout dot is detuned by charge noise. Majorana hybridization is only a second-order effect,²⁷ i.e. a minor correction of the error caused by the readout dot detuning.

One important practical conclusion drawn from the results of Fig. 4a is that the readout speed u_{max} should be fine tuned to a finite value (around 0.1Δ in this example) to minimize the readout error. In fact, the optimal readout speed can be found by using Eq. (11) and solving $d\epsilon/du_{\text{max}} = 0$, yielding

$$u_{\text{max}}^{(\text{opt})} = \frac{\sqrt{2}}{5^{1/4}} \sqrt{\sigma_{\text{noise}} \Delta}, \quad (12)$$

and the corresponding optimized (minimized) parity readout error is

$$\epsilon^{(\text{opt})} = \frac{\sqrt{5}}{4} \frac{\sigma_{\text{noise}}}{\Delta}. \quad (13)$$

A practical implication of our result (11) is that it provides a map of realistic parameter values that are required for a reasonably accurate parity readout experiment. This is shown in Fig. 5a, where the different regions correspond to different ranges of parity readout errors. For example, taking the realistic noise strength value^{32,42} $\sigma_{\text{noise}} = 1 \mu\text{eV}$, the figure indicates that an effective superconducting gap $\Delta \gtrsim 55 \mu\text{eV}$ and a tunnel pulse strength $\sim 10 \mu\text{eV}$ (corresponding to tunnel pulse duration ~ 100 ps) are required to have a parity readout error below 1 percent. This sounds in principle achievable, e.g., with the commonly used Al-coated III-V semiconductor nanowires^{49,50} where the Al gap is a few hundred microelectronvolts. Finally, the dashed line in Fig. 5a shows the optimal readout tunnel strength as a function of the induced gap Δ .

C. Charge relaxation due to phonon emission

In this section, we describe how parity readout error is induced due to spontaneous phonon emission, even at zero temperature. We use a simple example to illustrate

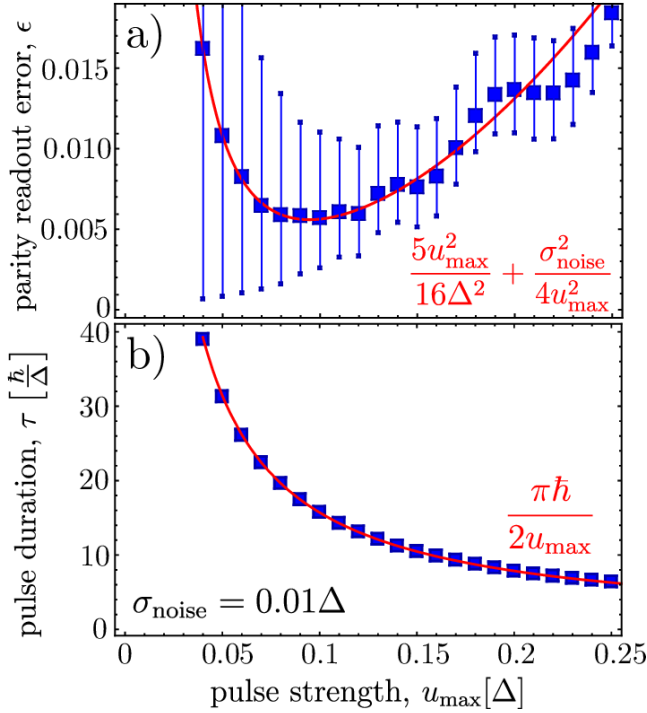


FIG. 4. Combined effects of tunnel pulse strength and slow charge noise on parity readout error. (a) Parity readout error averaged numerically for 5000 disorder realizations (boxes) and calculated analytically using perturbation theory (solid). (b) Optimal readout pulse duration obtained from the numerical optimization (boxes) and from the analytical estimate (solid).

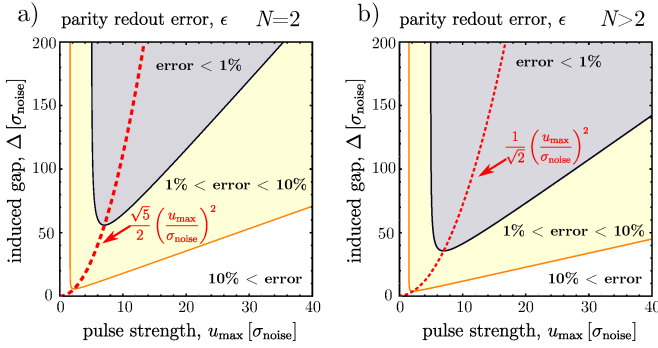


FIG. 5. Requirements on the system parameters to achieve certain parity readout error thresholds. Evaluated from the perturbative analytical result Eq. (11). The dashed red lines show the optimal pulse strength, derived by inserting the relations in Eqs. (12) and (28), respectively.

the role of phonons: a three-dimensional heterostructure based on InAs as the semiconducting material.^{51–53} Because of the available phonon states, the Rabi oscillation will not be fully coherent, but a charge relaxation process assisted by the spontaneous emission of a phonon will drive the system toward a quantum dot state that is a mixture of empty and filled, and hence will corrupt the parity-to-charge conversion process. We calculate the

phonon-induced error due to the deformation-potential electron-phonon coupling in this particular setup, finding that the error increases with increasing tunnel pulse strength as $\epsilon \propto u_{\max}^2$, similarly to the leakage error discussed in section III A, but we estimate that the phonon-induced error is much smaller than the leakage-induced error. We also note that the results of the phonon analysis depend qualitatively on the sample dimensionality and the electron-phonon interaction mechanism, we study only one example case here.

To illustrate the origin of the phonon-induced error, consider the case of zero temperature. First, take the case when the wire parity is even, corresponding to the level structure shown in Fig. 3a. In this case, when the tunnel pulse is turned on, the instantaneous energy eigenstates are the bonding $|b\rangle = \frac{1}{\sqrt{2}}(|e, 0\rangle - |o, 1\rangle)$ and antibonding $|a\rangle = \frac{1}{\sqrt{2}}(|e, 0\rangle + |o, 1\rangle)$ combinations of the basis states, which are separated by an energy gap of $2u_{\max}$, as shown in the inset of Fig. 6. The initial state $|e, 0\rangle$ is a balanced superposition of the bonding and antibonding states, that is, with a probability of 1/2 it occupies the excited state $|a\rangle$, and hence can relax to $|b\rangle$ by emitting a phonon. This relaxation process ends with the state $|b\rangle$ that has only $e/2$ charge on the readout dot, instead of charge e in the ideal case, implying that this phonon emission induces an error in the parity-to-charge conversion.

We describe the error due to this relaxation mechanism in two steps. First, we use the Bloch-Redfield master equation⁵⁴ to relate the energetically downhill $|a\rangle \mapsto |b\rangle$ relaxation rate Γ_{\downarrow} to the parity readout error ϵ . Second, we estimate the relaxation rate Γ_{\downarrow} induced by the deformation-potential electron-phonon interaction mechanism in an InAs heterostructure, using Fermi's Golden Rule, in a fashion similar to spin relaxation calculations in quantum dots.⁵⁵

To describe parity readout error due to relaxation, we focus on the two-dimensional subspace spanned by $|b\rangle$ and $|a\rangle$. The density matrix describing the initial state is $\rho(t=0) = |e, 0\rangle \langle e, 0|$. Parity readout error is the probability of finding the readout dot empty after the tunnel pulse duration $\tau = \pi\hbar/(2u_{\max})$, that is,

$$\epsilon = \text{Tr}[|e, 0\rangle \langle e, 0| \rho(\tau)]. \quad (14)$$

The time evolution of the density matrix is governed by the zero-temperature Bloch-Redfield equations:

$$\dot{\rho}_{aa}(t) = -\Gamma_{\downarrow}\rho_{aa}(t), \quad (15a)$$

$$\dot{\rho}_{bb}(t) = \Gamma_{\downarrow}\rho_{aa}(t), \quad (15b)$$

$$\dot{\rho}_{ba}(t) = \frac{2iu_{\max}}{\hbar}\rho_{ba}(t) - \frac{1}{2}\Gamma_{\downarrow}\rho_{ba}(t). \quad (15c)$$

Solving this and inserting the solution to Eq. (14) yields

$$\epsilon = \frac{1}{2} \left(1 - e^{-\pi\hbar\Gamma_{\downarrow}/(4u_{\max})} \right) \approx \frac{\hbar\pi}{8u_{\max}}\Gamma_{\downarrow}, \quad (16)$$

where we assumed that the exponent is much smaller than one, to be confirmed below.

Now, we determine the dependence of the $|a\rangle \mapsto |b\rangle$ relaxation rate Γ_\downarrow on the tunnel pulse strength u_{\max} . Since we envision that the inverse time scale of the readout (i.e., the charge Rabi frequency) is well below the THz range of typical optical-phonon frequencies, it is safe to assume that the phonon emitted upon the relaxation process is an acoustic one. We will use InAs as the exemplary host material, and for simplicity, we assume that the interaction between the electrons and the phonons is described by the deformation-potential mechanism, and that the acoustic phonons can be characterized as longitudinal and transverse bulk phonons. Note that under these assumptions, the transverse acoustic phonons do not cause volume change, and therefore they do not contribute to the deformation potential.

The electron-phonon Hamiltonian reads⁵⁶

$$H_{\text{e-ph}} = \Xi \text{Tr} \varepsilon(\mathbf{r}), \quad (17)$$

where Ξ is the deformation-potential constant, and $\varepsilon(\mathbf{r})$ is the strain tensor at the position \mathbf{r} of the electron. Using a single-electron basis formed by spatially localized states on the three sites (1, 2, and ‘dot’) of our model [Eq. (1)], the e-ph contribution to the globally even 4×4 sector of the 8×8 Hamiltonian reads:

$$H_{\text{e-ph}} = \begin{pmatrix} 0 & 0 & \frac{\tilde{\varepsilon}_1 + \tilde{\varepsilon}_2}{2} & 0 \\ 0 & \tilde{\varepsilon}_{\text{dot}} & 0 & \frac{\tilde{\varepsilon}_1 - \tilde{\varepsilon}_2}{2} \\ \frac{\tilde{\varepsilon}_1 + \tilde{\varepsilon}_2}{2} & 0 & 0 & 0 \\ 0 & \frac{\tilde{\varepsilon}_1 - \tilde{\varepsilon}_2}{2} & 0 & \tilde{\varepsilon}_{\text{dot}} \end{pmatrix} \quad (18)$$

where we have used the basis $|e, 0\rangle$, $|o, 1\rangle$, $|e', 0\rangle$, $|o', 1\rangle$. Furthermore, we assume that the deformation can be approximated as homogeneous within each site of the model, and hence the phonon-induced on-site energy shifts read, e.g., as $\tilde{\varepsilon}_1 \equiv \Xi \text{Tr}[\varepsilon(\mathbf{r}_1)]$.

As seen in Eq. (18), the phonon-induced on-site energy shifts on the two-site Kitaev chain do not give direct matrix elements within the relevant subspace spanned by $|e, 0\rangle$ and $|o, 1\rangle$, hence it is reasonable to neglect those and keep only the more important terms proportional to $\tilde{\varepsilon}_{\text{dot}}$. That is, for our purposes, the Hamiltonian is approximated as

$$H_{\text{e-ph}} \approx \tilde{\varepsilon}_{\text{dot}} |o, 1\rangle \langle o, 1| \equiv \frac{\tilde{\varepsilon}_{\text{dot}}}{2} (|a\rangle \langle b| + h.c.). \quad (19)$$

From this form, it is clear that the e-ph interaction induces a transition from $|a\rangle$ to $|b\rangle$. We calculate the rate of this transition from Fermi’s golden rule:

$$\Gamma_\downarrow = \frac{2\pi}{\hbar} \sum_{\mathbf{q}_f} |\langle b, \mathbf{q}_f | H_{\text{e-ph}} | a, 0 \rangle|^2 \delta(2u_{\max} - \hbar c_L q_f) \quad (20)$$

where 0 stands for the phonon vacuum, \mathbf{q}_f is the wave vector of the phonon emitted upon the transition, c_L is the speed of sound for longitudinal phonons, and we applied a linear, isotropic approximation for the dispersion of the acoustic phonons, $\omega_{\mathbf{q}} \approx c_L q$.

To evaluate the matrix element in Eq. (20), we recall that the e-ph Hamiltonian includes $\tilde{\varepsilon}_{\text{dot}} = \Xi \text{Tr}[\varepsilon(\mathbf{r}_{\text{dot}})]$,

where the strain tensor is related to the displacement field $\mathbf{u}(\mathbf{r})$ via $\varepsilon_{jk} = (\partial_j u_k + \partial_k u_j)/2$, and the displacement field of the longitudinal acoustic phonons is represented by the phonon creation and annihilation operators via

$$\mathbf{u}(\mathbf{r}) = \sum_{\mathbf{q}} \sqrt{\frac{\hbar}{2\rho V \omega_{\mathbf{q}}}} (a_{\mathbf{q}} + a_{-\mathbf{q}}^\dagger) e^{i\mathbf{q}\mathbf{r}} \mathbf{q}/q. \quad (21)$$

Here, ρ is the mass density of the host material and V is the volume of the host crystal. This expression allows a straightforward evaluation of Eq. (20) in the $V \rightarrow \infty$ limit, yielding

$$\Gamma_\downarrow = \frac{1}{\pi} \frac{\Xi^2 u_{\max}^3}{\rho \hbar^4 c_L^5}. \quad (22)$$

Using the result (22) in the error formula Eq. (16), we obtain

$$\epsilon = \frac{\Xi^2 u_{\max}^2}{8\rho \hbar^3 c_L^5}. \quad (23)$$

The error depends quadratically on the tunnel pulse strength u_{\max} , in a fashion similar to the leakage error evaluated in Eq. (10). In our numerical example however, the phonon-induced error is much smaller than the leakage error: for $\Delta = 100 \mu\text{eV}$ and $u_{\max} = 20 \mu\text{eV}$, the leakage error is $\epsilon \approx 1.25 \times 10^{-2}$, whereas for the InAs parameters $\rho = 5667 \text{ kg/m}^3$, $c_L = 4430 \text{ m/s}$, and $\Xi = 4.5 \text{ eV}$, the phonon-induced error is $\epsilon \approx 6 \times 10^{-5}$. More generally, the form of Eq. (23) corresponding to these InAs parameters reads

$$\epsilon = \left(\frac{u_{\max}}{2.61 \text{ meV}} \right)^2. \quad (24)$$

This result is shown as the solid line in Fig. 6. It is straightforward to generalize this result to the case of finite temperature, see Appendix D; the error for $T = 50 \text{ mK}$ is shown as the dashed line in Fig. 6, showing almost identical behavior to the zero-temperature case.

Our above analysis relied on a specific choice of material (InAs) and device structure (3D heterostructure). We expect that the results change qualitatively for different setups. A particularly relevant case, requiring a separate, detailed phonon analysis, is when the 1DTS is built as a combination of a quasi-1D semiconducting nanowire and an s-wave superconductor.^{6,16,57,58} Since in these devices, the nanowire is supported by a substrate, and (at least partially) clamped by the superconductor and the normal-metal contact electrodes, the acoustic phonon modes might be gapped, resulting in very long charge relaxation times, potentially eliminating the phonon hazard from the parity readout procedure based on charge Rabi oscillations.

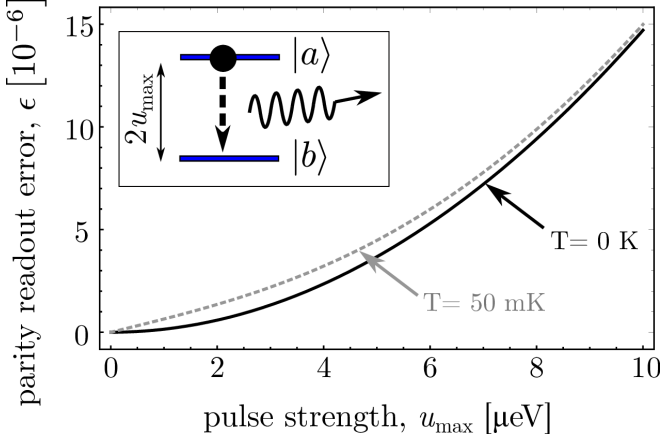


FIG. 6. Parity readout error due to phonon-mediated charge relaxation. At $T = 0$ K, the error is caused by spontaneous phonon emission (inset). At finite T , spontaneous and stimulated emission as well as absorption of thermal phonons contribute to the error.

IV. DISCUSSION

A. Parity readout in a long Kitaev chain in the ideal limit

The problem we have studied so far was based on a minimal model, the two-site Kitaev chain, which might be realized in a double quantum dot proximitized by a superconductor.^{27–29} To enable topologically protected qubits though, one needs to assemble longer chains, or consider proximitized quasi-one-dimensional nanostructures.² Motivated by these observations, we now generalize the two-site problem and here we consider a longer Kitaev chain, with $N > 2$ sites, coupled to the readout dot, as shown in Fig. 1c.

We still focus on the ideal Kitaev limit $v = \Delta$, but allow for disorder of the on-site energies the same way as we did before (see Eq. (1) and section III B). The Hamiltonian is $H = H_{\text{chain}} + H_{\text{dot}} + H_{\text{tun}}$, where

$$H_{\text{chain}} = \sum_{j=1}^N \varepsilon_j c_j^\dagger c_j \quad (25a)$$

$$+ \sum_{j=1}^{N-1} v(c_j^\dagger c_{j+1} + h.c.) + \Delta(c_j^\dagger c_{j+1}^\dagger + h.c.)$$

$$H_{\text{tun}} = u(t)(c_1^\dagger c_{\text{dot}} + c_N^\dagger c_{\text{dot}} + h.c.), \quad (25b)$$

and H_{dot} is defined in Eq. (1).

The key question is: how do the error mechanisms studied for the $N = 2$ case change as we consider longer chains? We investigate the same error mechanisms: (A) leakage, (B) incomplete charge Rabi oscillation, and (C) charge relaxation.

(A) The perturbative formula (10) can be straightforwardly extended to the $N > 2$ case, yielding a result that differs only in a prefactor from the $N = 2$ result of

Eq. (10):

$$\epsilon = \frac{1}{8} \left(\frac{u_{\text{max}}}{\Delta} \right)^2. \quad (26)$$

Appendix B contains the details of the derivation. The energy level diagrams depicting the process triggered by the readout tunnel pulse, for the $N = 3$ and $N = 4$ cases, are shown in Fig. 3c-f.

(B) The analytical estimate of the parity readout error due to slow charge noise and leakage, in the limit $\sigma_{\text{noise}} \ll u_{\text{max}} \ll \Delta$, was given for $N = 2$ in Eq. (11). This analytical result can be generalized to the $N > 2$ case:

$$\epsilon = \frac{1}{8} \left(\frac{u_{\text{max}}}{\Delta} \right)^2 + \frac{1}{4} \left(\frac{\sigma_{\text{noise}}}{u_{\text{max}}} \right)^2, \quad (N > 2). \quad (27)$$

That is, the error induced by the charge noise in the $N = 2$ case is different from the $N > 2$ cases, but in the latter cases it does not depend on the chain length N .

The error result (27), incorporating both leakage and incomplete Rabi oscillations, can be used to analytically estimate the optimal readout pulse strength and the corresponding minimal parity readout error. The formula for the optimal readout pulse strength reads

$$u_{\text{max}}^{(\text{opt})} = 2^{1/4} \sqrt{\sigma_{\text{noise}} \Delta}, \quad (28)$$

and the corresponding minimal parity readout error is

$$\epsilon^{(\text{min})} = \frac{1}{2\sqrt{2}} \frac{\sigma_{\text{noise}}}{\Delta}. \quad (29)$$

The length dependence of the minimal parity readout error, according to this analytical estimate, is shown as the red points in Fig. 7. The map of error thresholds corresponding to $N > 2$ is shown in Fig. 5b.

An important conclusion from Eq. (29) is that the optimal readout error as a function of chain length N saturates already at $N = 3$, and increasing the chain length does not bring any further improvement. This saturation of the readout error for increasing system size is in contrast to the length dependence of braiding-based quantum gates: in the latter case, increasing the system size can make the error exponentially suppressed.^{59,60} This observation highlights a practical difficulty of the parity readout scheme studied here. It will be an interesting extension of this work to study how the error in different parity readout schemes vary as the system size is increased, and whether there is a saturation effect similar to the one we have found. This task is particularly relevant for measurement-only topological quantum computing proposals,^{18,24} where quantum gates are performed via sequences of measurements, instead of braiding the anyonic defects.

To underpin the above analytical estimates, we have carried out numerical simulations of the parity readout process. From these simulations, we have obtained the numerical values of the parity readout error shown in Fig. 7 (blue squares), in good agreement with the analytical estimates (red points). The simulations follow the

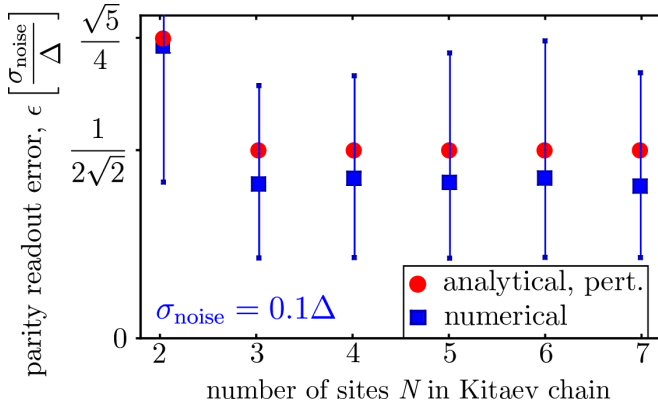


FIG. 7. Length dependence of optimal leakage error. Blue squares show the numerical results, red points show the perturbative analytical results (13) (for $N = 2$) and (29) (for $N > 2$).

scheme described in section III B. Error bars in Fig. 7 connect the 1st and 9th deciles of the $N_r = 5000$ different results corresponding to N_r different disorder realizations. For these length-dependent simulations, we have used the Bogoliubov de Gennes (BdG) formalism to compute the time evolution, instead of the direct Fock-space approach. We summarize the time-dependent BdG formalism in appendix E. The advantage of the BdG formalism over the Fock-space description is that the former requires diagonalizing $2(N+1) \times 2(N+1)$ matrices, whereas the latter requires diagonalizing $2^{N+1} \times 2^{N+1}$ matrices.

(C) The length of the chain has no effect in our model of the phonon-mediated charge relaxation. The reason is that the first-order correction of the energies of the chain's even and odd ground states due to the deformation potential is vanishing due to the usual topological protection, for any chain length $N \geq 2$. This is exemplified by the Hamiltonians in Eqs. (6) and (7), if ε_1 , ε_2 and ε_{dot} are interpreted as deformation-induced on-site energy shifts. As a consequence, the model and results of phonon-mediated charge relaxation hold for longer chains $N > 2$ as well. Similarly to the mechanisms (A) and (B), phonon-mediated charge relaxation is not mitigated by lengthening chain.

B. Smooth tunnel pulse leads to better readout

So far, we have assumed that the tunnel pulse enabling the parity-to-charge conversion has a square shape, see Fig. 1d and Eq. (8). It is natural to expect that the leakage error due to the sudden turn-on and turn-off of such a square pulse can be partially mitigated by using a smooth pulse shape instead. Here, we present numerical results that illustrate that this is indeed the case, and study how much is gained by using a smooth pulse.

In particular, here we use a smooth, exponential time-

dependent function, as shown in the inset of Fig. 8a:

$$u(t) = \begin{cases} u_{\text{max}} \chi(2t/\tau), & \text{if } t < \tau/2 \\ u_{\text{max}} (1 - \chi(2t/\tau)), & \text{if } t \geq \tau/2, \end{cases} \quad (30)$$

where the pulse shape function χ is defined as

$$\chi(x) = \frac{e^{-1/x}}{e^{-1/(1-x)} + e^{-1/x}}. \quad (31)$$

To realize a full Rabi oscillation, the duration τ of the pulse is chosen to be $\tau = \frac{\pi \hbar}{u_{\text{max}}}$. We solve the time-dependent Bogoliubov-de Gennes equation for this pulse shape numerically, in a similar fashion as described above, to calculate the disorder-averaged parity readout error for various chain lengths.

In Fig. 8a, we show the average parity readout error as a function of the tunnel pulse strength u_{max} , for a certain noise strength $\sigma_{\text{noise}} = 0.01\Delta$, in the case of a three-site Kitaev-chain. Comparing the results to those in Fig. 4a obtained for the square pulse, we note the following similarities: (i) There is an optimal parity readout error at a finite pulse strength; in Fig. 8a it is $\approx 0.25\Delta$. (ii) Away from this optimal pulse strength, the error is increasing for the same reasons as discussed in Sec. III. B and C.

One difference, however, is that the optimal parity readout error with the smooth pulse (Fig. 8a) is $\approx 5 \cdot 10^{-4}$, which is approximately five times smaller than in the case of the square pulse. To illustrate the generality of this performance gain of the smooth pulse, we plot the optimal parity readout error as a function of noise strength σ_{noise} in Fig. 8b, for two different chain lengths, comparing the performance of the square pulse and the smooth, exponential pulse. This plot shows that the using smooth pulse improves the parity readout error by a factor of ~ 2 -5. We also observed that using different smooth pulses, e.g., those with sine, sine-squared, etc., time dependence, we obtain almost the same optimized parity readout error as with the exponential pulse.

These results imply that the adiabatic errors of parity readout in this setting can be significantly reduced by using smooth tunnel pulses instead of square pulses.

C. Refinements of the noise model

Our work provides an extension of earlier theory works studying the effect of charge noise and phonons on readout of Majorana-based qubits. Karzig et al.¹⁸ treated charge noise phenomenologically (see their Eqs. (C21)-(C23)). Similarly to Knapp et al.²¹ (see their Eqs. (43)-(44)), both of these works studied noise effects that are beneficial for readout. Munk et al.²² provided a perturbative analysis in equilibrium, which indicates that the readout visibility and fidelity are influenced by the entanglement of the device electrons and their quantum-mechanical environment (see their section IV. B). Hyart et al.²³ describe a flux-controlled setup, and analyze the readout error due to photon shot noise of the readout cavity, a mechanism which is indeed practically relevant,

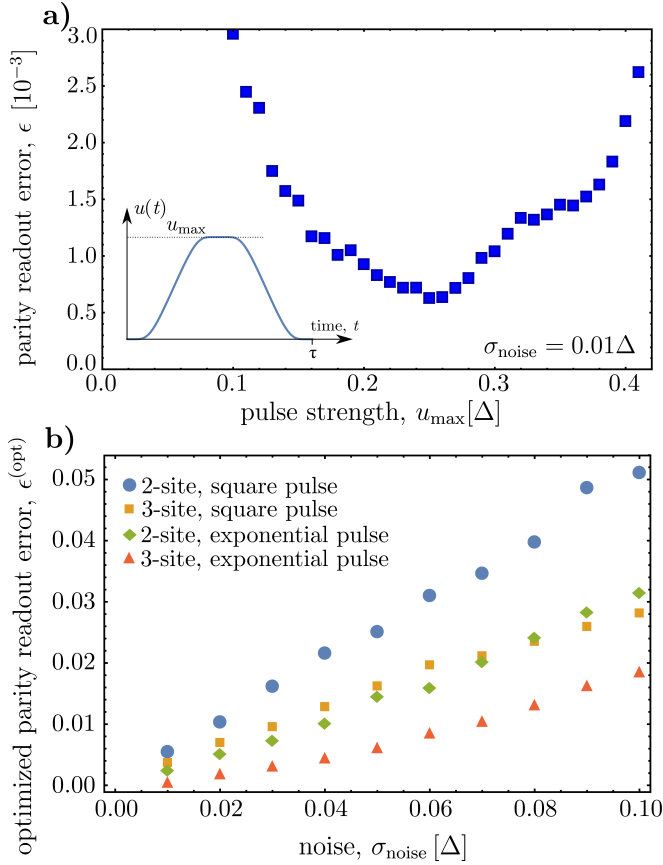


FIG. 8. Effect of the shape of tunnel pulse. (a) Parity readout error averaged over numerically for 1000 disorder realizations (boxes) in case of exponential-shape tunnel pulse (inset) and three-site Kitaev chain. (b) Optimized parity readout error as a function of noise strength for two- and three-site Kitaev chain in case of squared-shape and exponential-shape tunnel pulse.

although only indirectly related to the physics of Majorana zero modes (see their Appendix B). Munk et al.³⁸ and Steiner et al.³⁷ investigated the effect of noise on Majorana readout induced by the measurement device.

We think that our quantitative analysis of readout error due to leakage, charge noise and phonons, which is based on transparent non-equilibrium minimal models possessing only the key physical ingredients, will serve as important benchmarks for future works both in theory and experiment. Nevertheless, we envision that developing and understanding a realistic parity-readout experiment will require a more elaborate theoretical treatment, in which the electronic-structure models and the noise models applied in the present work are refined. For example, a distinct type of readout error might be caused by the high-frequency component of charge noise,^{61–63} which was neglected in our present work. Regardless of the noise model used, as long as noise is classical, the way to calculate readout error is similar to the way we used here: due to noise, the charge of the readout dot becomes a random variable, and the task is to connect

the statistical characteristics of the noise to the probability distribution of the measured charge. Since the charge here is a binary variable, i.e., its measured value is either 0 or 1, its distribution is completely characterized by its average, which we calculated in the present work for the special case of quasistatic charge noise.

D. Potential extensions of the phonon analysis

In the phonon analysis of section III C, we considered the deformation-potential electron-phonon interaction mechanisms. However, theoretical⁵⁵ and experimental^{64,65} results indicate that the piezoelectric electron-phonon interaction is also important, and can even dominate, in semiconductors without inversion symmetry, such as the materials InAs and InSb frequently used in engineered topological superconductors.^{6,10} Evaluating the effect of piezoelectricity on the readout procedure studied here is therefore an important future task. In principle, piezoelectric effects could be avoided by using host materials having inversion symmetry, such as silicon or germanium.

A further interesting extension of the present work could aim at a more balanced description of the electron-phonon interaction. The key observation is that in our model, phonons play two different roles, and these two roles are represented as independent ingredients in the model, even though they arise from the same microscopic origin. First, the e-ph coupling provides the glue of the Cooper pairs, and hence the e-ph coupling is hidden in the effective superconducting gap Δ . Second, the e-ph coupling contributes to the charge relaxation process leading to parity readout error. Treating these two roles of the e-ph coupling on an equal footing would be an elegant and desirable extension of our work. We speculate that the semi-phenomenological model we used in this work might even gain a microscopic foundation, e.g., in the case of superconductor-semiconductor heterostructures, where the gap could mostly be determined by the phonons in the superconductor, whereas the relaxation could be dominated by the semiconductor phonons.

E. Parity readout as a generalized measurement

In this work, we characterized the parity readout error in terms of a single number between 0 and 1. A more thorough description of the readout procedure can be given using generalized POVM measurements.⁶⁶ The future extension of this work that includes this refinement can provide a useful tool in post-processing the measured data in quantum-information experiments.

V. CONCLUSIONS

In conclusion, we have studied error mechanisms affecting the readout of a Majorana qubit in a one-dimensional topological superconductor. We describe (i) leakage due to a strong readout tunnel pulse, (ii) incomplete charge Rabi oscillations due to slow charge noise, and (iii) charge relaxation due to phonon emission and absorption. Using minimal models based on the Kitaev chain, we calculate the readout error for these mechanisms.

Our work highlights and quantifies a practical difficulty with the Rabi-oscillation-based parity readout scheme we studied here. Namely, the readout process does not enjoy the same topological protection as the braiding-based quantum gates, i.e., the readout error does saturates to a nonzero value as the chain length increases. This issue requires careful consideration, if this measurement scheme is to be used in practical quantum-information experiments, especially for measurement-only quantum computing.

We also provide guidelines for experiments: given a certain level of charge noise and a certain phonon environment, what are the requirements to perform a readout experiment with a certain small readout error? For an example case where the device is based on a three-dimensional InAs nanostructure, we estimate that the error is caused mainly by leakage and slow charge noise, and phonon effects are negligible. For this case, we provide analytical formulas on optimal readout errors and how to achieve those. We expect that these results contribute to the fundamental understanding of topological qubit readout, and provide practical guidance for near-term experiments aiming at topological qubit demonstrations.

ACKNOWLEDGMENTS

We acknowledge useful discussions with J. Asbóth, M.-S. Choi, V. Derakhshan, J. König, R. Lutchyn, and G. Steffensen. This research was supported by the National Research Development and Innovation Office of Hungary within the Quantum Technology National Excellence Program (Project No. 2017-1.2.1-NKP-2017-00001), grant FK124723 and BME-Nanotechnology FIKP grant (BME FIKP-NAT). This work was completed in the ELTE Institutional Excellence Program (1783-3/2018/FEKUTSRAT) supported by the Hungarian Ministry of Human Capacities.

Appendix A: Low-energy description of parity-to-charge conversion

In section II, we described the parity-to-charge conversion mechanism in terms of the complete Fock-space Hamiltonian. Here, we provide an insightful, approximate low-energy description.¹⁵ Even though the low-

energy nature of this approximation implies that it cannot directly be used to describe the leakage error, it is useful to describe the charge-noise induced and phonon-induced errors.

The short informal summary of this low-energy picture, exemplified using the two-site Kitaev chain, is as follows. The ideal Kitaev chain hosts two zero-energy Majorana modes, which can be combined into a single zero-energy fermionic mode, such that the occupation of this mode (zero or one) corresponds to the ground-state fermionic parity (odd or even). On the one hand, if this fermionic mode is empty in the initial state (for $N = 2$, this is the odd state), then this mode as well as the readout dot will remain empty at the end of the readout procedure. On the other hand, if this fermionic mode is occupied in the initial state (for $N = 2$, this is the even state), then this excitation will be transferred to the dot by the end of the readout tunnel pulse, leaving the fermionic mode empty but making the dot occupied.

To formalize this, we rewrite the terms of the chain Hamiltonian H_{chain} and the chain-dot tunneling Hamiltonian H_{tun} in terms of the Majorana operators

$$\gamma_{1A} = c_1^\dagger + c_1, \quad (\text{A1})$$

$$\gamma_{1B} = i(c_1 - c_1^\dagger), \quad (\text{A2})$$

with analogous definitions for site 2. In this Majorana representation, the Hamiltonians read

$$H_{\text{chain}} = 2\Delta\gamma_{1B}\gamma_{2A}, \quad (\text{A3})$$

$$H_{\text{tun}} = \frac{u(t)}{2} [(\gamma_{1A} + i\gamma_{1B})c_{\text{dot}} + (\gamma_{2A} + i\gamma_{2B})c_{\text{dot}} + h.c.] \quad (\text{A4})$$

One observation is that γ_{1A} and γ_{2B} are absent from H_{chain} . This implies that the nonlocal zero-energy mode

$$d^\dagger = \frac{1}{2}(\gamma_{1A} + i\gamma_{2B}). \quad (\text{A5})$$

can be considered a low-energy eigenmode of H_{chain} , and any further Majorana operators are related to high-energy excitations and hence can be neglected in a low-energy approximation as long as $u(t) \ll \Delta$. With this reasoning, we truncate the tunneling Hamiltonian to low energies, yielding the following approximation:

$$H_{\text{tun}} \approx u(t)(d^\dagger c_{\text{dot}} + h.c.). \quad (\text{A6})$$

The final expression in Eq. (A6) reveals the simple picture anticipated in the previous paragraph.

It is straightforward to generalize these considerations for any 1DTS, by using the actual Majorana zero modes instead of γ_{1A} and γ_{2B} . However, in such a generalized scenario, the electron transfer probability can be finite for both the even and odd initial states. To illustrate this, let us generalize our previous calculations by modifying the tunnelling Hamiltonian to include two independent, complex-valued tunneling amplitudes:

$$H'_{\text{tun}} = \left(u_1 c_1^\dagger c_{\text{dot}} + h.c.\right) + \left(u_2 c_2^\dagger c_{\text{dot}} + h.c.\right) \quad (\text{A7})$$

Expressing this generalized tunneling Hamiltonian at low energies, in terms of the zero-energy fermionic mode d^\dagger , we find

$$H'_{\text{tun}} \approx \frac{u_1 + u_2}{2} d^\dagger c_{\text{dot}} + \frac{u_1 - u_2}{2} d c_{\text{dot}} + h.c. \quad (\text{A8})$$

This reveals that fine tuning $u_1 = u_2$ is required to completely forbid tunneling for the odd initial state.

How is this fine-tuning requirement relevant for experiments? Let us exemplify this via the 1DTS system based on a semiconductor nanowire proximitized by an s -wave superconductor.^{57,58} Here, a finite magnetic field is required to induce the 1DTS state. The presence of this magnetic field implies that time-reversal symmetry is broken, so in general, tunnel amplitudes in a loop topology (see, e.g., Fig. 1b,c) are complex-valued. In the setting considered here, where the tunnel amplitudes u_1 and u_2 assist the tunneling process, a magnetic flux piercing the loop formed by the wire and the dot should be fine-tuned such that the complex phases of u_1 and u_2 are the same. Of course, the absence of this fine tuning is not detrimental for the readout process, since the effective fermionic tunneling amplitude $(u_1 - u_2)/2$ for the odd state is in general different from the amplitude $(u_1 + u_2)/2$ for the even state; fine tuning is required only to optimize the contrast between the two initial states.

Appendix B: Perturbative calculation for the leakage-induced parity readout error

1. Two-site Kitaev chain

Here, we calculate the leakage-induced parity readout error in a two-site Kitaev chain (ideal Kitaev limit, $v = \Delta$) during the readout protocol described in section II. We are focusing only the perturbative limit, when the strength of the readout tunnel pulse u_{max} is much less than the effective superconducting gap of the Kitaev chain, i.e. $u_{\text{max}} \ll \Delta$. We will show that the parity readout error is well approximated by the simple result in Eq. (10).

Without the tunnel pulse, the chain is uncoupled from the dot, and it has four energy eigenstates: $|e\rangle$ and $|o\rangle$ at energy $-\Delta$, and $|e'\rangle$ and $|o'\rangle$ at Δ . Since the total parity is conserved during the readout process, we will separately investigate the cases where the parity is even or odd.

First, we consider the odd subspace, see Eq. (7). Here, the Hamiltonian $H_0 = H_{\text{chain}} + H_{\text{dot}}$ of the disjoint system, up to a global energy shift, reads

$$H_0^{\text{odd}} = 2\Delta (|e', 1\rangle \langle e', 1| + |o', 0\rangle \langle o', 0|), \quad (\text{B1})$$

whereas the tunneling Hamiltonian is

$$H_{\text{tun}}^{\text{odd}} = u_{\text{max}} (|o', 0\rangle \langle e', 1| - |e, 1\rangle \langle o', 0| + h.c.). \quad (\text{B2})$$

From the latter we see that the initial state $|o, 0\rangle$ does not couple to other states, hence the readout dot remains

empty during the readout, $P_{1\leftarrow o}(t) = 0$. This is also depicted in the level diagram in Fig.3b.

Second, we consider the even subspace. Here, the Hamiltonian $H_0 = H_{\text{chain}} + H_{\text{dot}}$ of the disjoint system, see Eq. (6), up to a global energy shift, reads

$$H_0^{\text{even}} = 2\Delta (|e', 0\rangle \langle e', 0| + |o', 1\rangle \langle o', 1|), \quad (\text{B3})$$

and the tunneling Hamiltonian is

$$H_{\text{tun}}^{\text{even}} = u_{\text{max}} (|o, 1\rangle \langle e, 0| + |o, 1\rangle \langle e', 0| + h.c.). \quad (\text{B4})$$

The first term and its h.c. induces the charge Rabi oscillations allowing for the parity-to-charge conversion. The second term and its h.c. induces leakage from the relevant subspace, and this leakage leads to imperfect readout.

Treating $H_{\text{tun}}^{\text{even}}$ as the perturbation, we use perturbation theory to obtain the eigenstates $|j\rangle$ ($j \in \{1, 2, 3, 4\}$) of $H^{\text{even}} = H_0^{\text{even}} + H_{\text{tun}}^{\text{even}}$ and the energies E_j up to second order in u_{max}/Δ . If the initial state is $|e, 0\rangle$, then the probability that the QD is occupied after a time t is

$$P_{1\leftarrow e}(t) = |\langle o, 1| U(t) |e, 0\rangle|^2 + |\langle o', 1| U(t) |e, 0\rangle|^2 \quad (\text{B5})$$

where the time-evolution operator is $U(t) = e^{-iE_j t/\hbar} |j\rangle \langle j|$. In Eq. (B5), the second term vanishes because the state $|o', 1\rangle$ is not populated during the time evolution of $|e, 0\rangle$. To evaluate $P_{1\leftarrow e}$ in Eq. (B5), we drop those terms of the projectors $|j\rangle \langle j|$ in the propagator $U(t)$ that are beyond second order in u_{max}/Δ , yielding

$$P_{1\leftarrow e}(t) \approx \left[1 - \frac{5}{16} \left(\frac{u_{\text{max}}}{\Delta} \right)^2 \right] \sin^2 \left(\frac{u_{\text{max}}}{\hbar} t \right). \quad (\text{B6})$$

This expression reaches its maximum at $t = \frac{\pi\hbar}{2u_{\text{max}}}$. Hence, the leakage does not change the optimal duration of the tunnel pulse. This maximum of $P_{1\leftarrow e}(t)$ is below 1, hence the readout is imperfect, and the corresponding parity readout error can be read off from Eq. (B6), and is given by Eq. (10).

2. Three-site or longer Kitaev chains

In a three-site or longer Kitaev chain, there are more than two high-energy states, see Fig. 3c-f. However, in the ideal Kitaev limit studied here, only two of them, $|o'\rangle$ and $|e'\rangle$, are coupled to the low energy ground states $|o\rangle$ and $|e\rangle$, by the readout pulse. We restrict our calculation to these four states and show that the leakage-induced parity readout error for $N > 2$ is given by Eq. (26).

In case of a three-site chain in the ideal Kitaev limit, the initial state $|e, 0\rangle$ remains unchanged (see Fig. 3c), whereas the initial state $|o, 0\rangle$ evolves into $|e, 1\rangle$ due to the readout pulse (see Fig. 3d). The coupling to the high-energy states makes readout imperfect, and leads to a nonzero parity readout error. The unperturbed Hamiltonian in the odd subspace is the same as in Eq. (B1),

but the perturbation has a different form, namely

$$H_1^{\text{odd}} = u_{\text{max}} (|e, 1\rangle \langle o, 0| + h.c.) + \frac{u_{\text{max}}}{\sqrt{2}} (|e, 1\rangle \langle o', 0| + |o, 0\rangle \langle e', 1| + h.c.). \quad (\text{B7})$$

Following the method described in the previous subsection, we can calculate the dot occupation at time t , and find

$$P_{1 \leftarrow o}(t) = |\langle e, 1| U(t) |o, 0\rangle|^2 + |\langle e', 1| U(t) |o, 0\rangle|^2 \quad (\text{B8})$$

$$= \sin^2 \left(\frac{tu_{\text{max}}}{\hbar} \right) - \frac{u_{\text{max}}^2}{8\Delta^2} + \frac{u_{\text{max}}^2}{16\Delta^2} \cos \left(\frac{tu_{\text{max}}}{\hbar} \right)$$

$$\times \left\{ 6 \cos \left(\frac{tu_{\text{max}}}{\hbar} \right) - 4 \cos \left[\frac{t}{2\hbar\Delta} (4\Delta^2 + u_{\text{max}}^2) \right] \right\}.$$

This function has a maximum at $t = \frac{\pi\hbar}{2u_{\text{max}}} + \mathcal{O} \left(\frac{u_{\text{max}}\hbar}{\Delta^2} \right)$, so the optimal length of the pulse gets a small correction, compared to the leakage-free case. The leading-order value $\frac{u_{\text{max}}^2}{8\Delta^2}$ of the parity readout error is coming from the maximal value of Eq. B8.

In the even subspace, the unperturbed Hamiltonian is that in Eq. (B3), but the perturbation is

$$H_{\text{tun}}^{\text{even}} = u_{\text{max}} \left(\frac{1}{\sqrt{2}} |e, 0\rangle \langle o', 1| + |o', 1\rangle \langle e', 0| + h.c. \right) \quad (\text{B9})$$

The readout tunnel pulse gives no matrix element between the ground states, therefore the initial state $|e, 0\rangle$ is stationary if we disregard higher-energy states. In contrast to the 2-site case, the state $|e, 0\rangle$ is not decoupled from the other states, but is coupled to high-energy states. This feature provides a small but finite probability for the dot being occupied at the end of the tunnel pulse:

$$P_{1 \leftarrow e}(t = \pi/(2u_{\text{max}})) = \frac{u_{\text{max}}^2}{8\Delta^2}. \quad (\text{B10})$$

Hence, we conclude that the parity readout error is indeed given by Eq. (26) in this case.

We can generalize this result for $N > 3$. Whenever N is odd, then the leading-order dynamics is that the initial state $|e, 0\rangle$ evolves into the state $|o, 1\rangle$ and hence the charge of the dot changes from 0 to 1, whereas the initial state $|o, 0\rangle$ remains unchanged. Coupling to the high-energy states spoils the perfect parity-to-charge conversion. The level diagrams of the most relevant states are analogous to those in Figs. 3c and d, and this implies that the parity readout error in the perturbative limit is given by Eq. (26). Furthermore, the same conclusion can be derived for the cases when N is even and $N > 3$.

Appendix C: Perturbative calculation of the parity readout error due to slow charge noise

In the main text, we have provided analytical perturbative results, Eqs. (11) and (27) for the parity readout

error in the presence of slow charge noise. Here we provide the details leading to those results.

As discussed in the main text, we consider uncorrelated quasi-static on-site energy noise (disorder) on the chain sites as well as on the dot, and represent disorder with Gaussian random variables with standard deviation σ_{noise} . We consider a specific perturbative limit, defined by $\sigma_{\text{noise}} \ll u_{\text{max}} \ll \Delta$. We will show that the value of noise-induced parity readout error is $\frac{\sigma_{\text{noise}}^2}{4u_{\text{max}}^2}$, irrespective of the chain length N .

Recall that the on-site energies of the QDs in the Kitaev chain are denoted by ε_i , where $i \in \{1, \dots, N\}$, furthermore, the on-site energy of the readout dot is denoted by ε_{dot} . The Hamiltonian of the globally even sector, projected onto the 2×2 subspace spanned by the ground states $|e, 0\rangle$ and $|o, 1\rangle$:

$$H = \varepsilon_{\text{dot}} |o, 1\rangle \langle o, 1| + u_{\text{max}} (|e, 0\rangle \langle o, 1| + h.c.), \quad (\text{C1})$$

where only the onsite-energy of the dot appears. Note that for simplicity, we use a notation corresponding to an even chain length N , but all conclusions are also valid for an odd N by the replacements $e \leftrightarrow o$.

If the initial state is $|e, 0\rangle$, then the dot occupation probability after a time t is

$$P_{1 \leftarrow e}(t) = \frac{4u_{\text{max}}^2}{4u_{\text{max}}^2 + \varepsilon_{\text{dot}}^2} \sin^2 \left(\frac{1}{2\hbar} t \sqrt{4u_{\text{max}}^2 + \varepsilon_{\text{dot}}^2} \right) \quad (\text{C2})$$

and $P_{0 \leftarrow e}(t) = 1 - P_{1 \leftarrow e}$. Taking the disorder-averaged value $\bar{P}_{0 \leftarrow e}$ of the probability $P_{0 \leftarrow e}(t)$ at time $t = \pi\hbar/(2u_{\text{max}})$, we find

$$\bar{P}_{0 \leftarrow e} = \int_{-\infty}^{\infty} d\varepsilon_{\text{dot}} P_{0 \leftarrow e} \left(t = \frac{\pi\hbar}{2u_{\text{max}}} \right) \frac{e^{-\frac{\varepsilon_{\text{dot}}^2}{2\sigma_{\text{noise}}^2}}}{\sqrt{2\pi}\sigma_{\text{noise}}}$$

$$\approx \frac{\sigma_{\text{noise}}^2}{4u_{\text{max}}^2}. \quad (\text{C3})$$

In the last approximation, we applied the hierarchy of the parameters $\sigma_{\text{noise}} \ll u_{\text{max}} \ll \Delta$.

Appendix D: Charge relaxation due to phonon emission at finite temperature

In section III C of the main text, we presented results for the parity readout error due to phonon-mediated inelastic processes. There, we focused on the zero-temperature case. Here, we provide details of the calculation of the finite-temperature case. Compared to the zero temperature limit where only spontaneous emission of phonons influence the parity-to-charge conversion, here we discuss the finite-temperature effects of stimulated emission and absorption of phonons as well.

First, we generalize Eq. (16) to derive the relation between the parity readout error ϵ and the inelastic rates. In this case, we have an energetically downhill rate Γ_{\downarrow} , accounting for phonon emission and de-excitation from

state $|a\rangle$ to state $|b\rangle$, and an uphill rate Γ_\uparrow , accounting for phonon absorption and excitation from $|b\rangle$ to $|a\rangle$. The time evolution of the density matrix is described by the Bloch-Redfield equation:⁵⁴

$$\dot{\rho}_{bb}(t) = -\Gamma_\uparrow \rho_{bb}(t) + \Gamma_\downarrow \rho_{aa}(t), \quad (\text{D1})$$

$$\dot{\rho}_{aa}(t) = \Gamma_\uparrow \rho_{bb}(t) - \Gamma_\downarrow \rho_{aa}(t), \quad (\text{D2})$$

$$\dot{\rho}_{ab}(t) = \frac{2iu_{\max}}{\hbar} \rho_{ab}(t) - \frac{1}{T_2} \rho_{ab}(t), \quad (\text{D3})$$

where $\frac{1}{T_2} = \frac{\Gamma_\uparrow + \Gamma_\downarrow}{2}$. Initially, our state is $|e, 0\rangle$, so $\rho_{bb}(0) = \rho_{aa}(0) = \rho_{ab}(0) = \rho_{ba}(0) = \frac{1}{2}$. The parity readout error ϵ is the probability of finding the readout dot empty after a time $t = \tau_{\text{ideal}} = \frac{\hbar\pi}{2u_{\max}}$, that is,

$$\epsilon = \frac{\rho_{bb}(\tau_{\text{ideal}}) + \rho_{ab}(\tau_{\text{ideal}}) + \rho_{ba}(\tau_{\text{ideal}}) + \rho_{aa}(\tau_{\text{ideal}})}{2} \quad (\text{D4})$$

The trace of the density matrix does not change in time, i.e., $\rho_{bb}(t) + \rho_{aa}(t) = 1$. Solving the differential equation of $\rho_{ba}(t)$, we obtain

$$\rho_{ba}(t) = \frac{1}{2} e^{\frac{2iu_{\max}t}{\hbar} - \frac{t}{T_2}}. \quad (\text{D5})$$

Then, we substitute this solution to Eq. (D4), insert $t = \tau_{\text{ideal}}$, and thereby obtain, as a generalization of Eq. (16)

$$\epsilon = \frac{1}{2} \left[1 - e^{-\frac{\tau_{\text{ideal}}}{T_2}} \right] \approx \frac{\tau_{\text{ideal}}}{2T_2} = \frac{\hbar\pi (\Gamma_\uparrow + \Gamma_\downarrow)}{8u_{\max}}. \quad (\text{D6})$$

We also need the finite-temperature values of the transition rates. As usual, the rate of stimulated emission and the rate of absorption are both equal to the rate of spontaneous emission multiplied by the Bose-Einstein function at the transition energy, that is, $n_{\text{BE}}(2u_{\max}, T) = \left(e^{\frac{2u_{\max}}{k_B T}} - 1 \right)^{-1}$. In formulas, this means

$$\Gamma_\downarrow(T) = \Gamma_\downarrow(T=0) [1 + n_{\text{BE}}(2u_{\max}, T)], \quad (\text{D7})$$

$$\Gamma_\uparrow(T) = \Gamma_\downarrow(T=0) n_{\text{BE}}(2u_{\max}, T). \quad (\text{D8})$$

Combining these expressions with Eq. (D6), we obtain the parity readout error as

$$\epsilon = \frac{1}{4} T_{\text{Rabi}} (\Gamma_\uparrow + \Gamma_\downarrow) = \frac{\Xi^2 u_{\max}^2}{8\rho\hbar^3 c_L^5} \coth\left(\frac{u_{\max}}{k_B T}\right). \quad (\text{D9})$$

For a 3D bulk InAs device, see material parameters in the main text, this result reads as

$$\epsilon = \left(\frac{u_{\max}}{2.61 \text{ meV}} \right)^2 \coth\left(\frac{u_{\max}}{k_B T}\right). \quad (\text{D10})$$

In Fig. 6, we compare the phonon-induced parity readout error at zero temperature (solid black) and at $T = 50$ mK (dashed gray), corresponding to the energy scale $k_B T \approx 4.3 \mu\text{eV}$.

Appendix E: Bogoliubov-de Gennes formalism for dynamics

In section IV A, we have considered the dependence of the parity readout error ϵ on the chain length N . The numerical results in Fig. 7 are obtained by applying the Bogoliubov-de Gennes (BdG) formalism to describe the dynamics⁶⁷ of the system. Here, we outline this formalism. For concreteness, we describe the special case when the readout dot is coupled to the two-site Kitaev chain, $N = 2$; generalization is straightforward.

The setup is modelled by the time-dependent Hamiltonian $H(t)$ in Eq. (1). Once we define the column vector $\tilde{\mathbf{c}}$ of the local fermionic operators via

$$\tilde{\mathbf{c}} = \begin{pmatrix} c_1 \\ c_2 \\ c_{\text{dot}} \\ c_1^\dagger \\ c_2^\dagger \\ c_{\text{dot}}^\dagger \end{pmatrix}, \quad (\text{E1})$$

we can rearrange the Hamiltonian H as

$$H(t) = \frac{1}{2} \tilde{\mathbf{c}}^\dagger \mathcal{H}(t) \tilde{\mathbf{c}} + \frac{\epsilon_1 + \epsilon_2 + \epsilon_{\text{dot}}}{2}. \quad (\text{E2})$$

Here, we have introduced the BdG matrix via

$$\mathcal{H}(t) = \begin{pmatrix} \epsilon_1 & v & u(t) & 0 & \Delta & 0 \\ v & \epsilon_2 & u(t) & -\Delta & 0 & 0 \\ u(t) & u(t) & \epsilon_{\text{dot}} & 0 & 0 & 0 \\ 0 & -\Delta & 0 & -\epsilon_1 & -v & -u(t) \\ \Delta & 0 & 0 & -v & -\epsilon_2 & -u(t) \\ 0 & 0 & 0 & -u(t) & -u(t) & -\epsilon_{\text{dot}} \end{pmatrix} \quad (\text{E3})$$

and the dagger in $\tilde{\mathbf{c}}^\dagger$ implies element-wise hermitian conjugation as well as transposing the column vector to transform it into a row vector.

The form of $\mathcal{H}(t)$ is specified by the requirement that it is particle-hole symmetric for all times t , that is,

$$\mathcal{P} \mathcal{H}(t) \mathcal{P}^{-1} = -\mathcal{H}(t), \quad (\text{E4})$$

where $\mathcal{P} = \sigma_x K$ is the canonical particle-hole transformation, with σ_x being the first Pauli matrix acting on the Nambu (particle-hole) degree of freedom, and K is complex conjugation.

Recall that in the readout protocol, initially there is no tunneling between the Kitaev chain and the readout dot, $u(t=0) = 0$. The corresponding Hamiltonian (BdG matrix) will be denoted as H_i (\mathcal{H}_i). When the tunnel pulse is switched on for $0 < t < \tau$, then $u(t) = u_{\max}$. The corresponding Hamiltonian (BdG matrix) will be denoted as H_f (\mathcal{H}_f).

Our goal is to describe the time evolution of the expectation value of an observable, for two different initial states. Our observable is the dot occupation $n_{\text{dot}} = c_{\text{dot}}^\dagger c_{\text{dot}}$, since this is used to characterize the parity readout error. The two different initial states are the even and odd ground states of the chain, with empty dots in both

cases. To be able specify the initial states more precisely, we first discuss the relation between the many-body energy eigenstates and the BdG matrix.

By solving the eigenvalue problem of the initial BdG matrix \mathcal{H}_i , we can find the six eigenvalues λ_i and the corresponding eigenvectors (column vectors) ϕ_i , with $i = 1, 2, \dots, 6$. Due to the particle-hole symmetry of the BdG matrix, it is possible (and convenient) to order the eigenvalues such that $\lambda_1, \lambda_2, \lambda_3 > 0$ and $\lambda_4 = -\lambda_1$, $\lambda_5 = -\lambda_2$, $\lambda_6 = -\lambda_3$. We can also choose the eigenvectors such that $\phi_4 = \mathcal{P}\phi_1$, $\phi_5 = \mathcal{P}\phi_2$, $\phi_6 = \mathcal{P}\phi_3$.

Using the eigenvectors ϕ_i , we can express the unitary diagonalizer of \mathcal{H}_i via

$$U_{\text{diag}} = \begin{pmatrix} \phi_1^\dagger \\ \dots \\ \phi_6^\dagger \end{pmatrix}, \quad (\text{E5})$$

and the quasiparticle operators via

$$\tilde{\mathbf{d}} = U_{\text{diag}} \tilde{\mathbf{c}}. \quad (\text{E6})$$

The Hamiltonian H_i is diagonalized, or in other words, it is written as the Hamiltonian of non-interacting quasiparticles, as

$$H_i = \frac{1}{2} \tilde{\mathbf{d}}^\dagger \mathcal{H}_i^{(\text{d})} \tilde{\mathbf{d}} + \frac{\epsilon_1 + \epsilon_2 + \epsilon_{\text{dot}}}{2}. \quad (\text{E7})$$

with

$$\mathcal{H}_i^{(\text{d})} = \text{diag}(\lambda_1, \lambda_2, \lambda_3, -\lambda_1, -\lambda_2, -\lambda_3). \quad (\text{E8})$$

Due to the particle-hole symmetry exploited above, we can label the elements of the vector $\tilde{\mathbf{d}}$ as

$$\tilde{\mathbf{d}} = \begin{pmatrix} d_1 \\ d_2 \\ d_3 \\ d_1^\dagger \\ d_2^\dagger \\ d_3^\dagger \end{pmatrix}. \quad (\text{E9})$$

Recall that our goal is to calculate the time dependence of the dot occupation, e.g.,

$$P_{1 \leftarrow e}(t) = \langle \Psi_e | [\tilde{\mathbf{c}}(t)]_6 [\tilde{\mathbf{c}}(t)]_3 | \Psi_e \rangle \quad (\text{E10})$$

where $[\dots]_j$ is the j th component of the vector, $|\Psi_e\rangle$ denotes the even-parity initial state, and the elements of the vector $\tilde{\mathbf{c}}(t)$ are the elements of the vector $\tilde{\mathbf{c}}$, transformed to the Heisenberg picture:

$$\begin{aligned} \tilde{\mathbf{c}}(t) &= e^{iH_f t/\hbar} \tilde{\mathbf{c}} e^{-iH_f t/\hbar} = \\ &= e^{i\frac{1}{2\hbar} \tilde{\mathbf{c}}^\dagger \mathcal{H}_f \tilde{\mathbf{c}} t} \tilde{\mathbf{c}} e^{-i\frac{1}{2\hbar} \tilde{\mathbf{c}}^\dagger \mathcal{H}_f \tilde{\mathbf{c}} t} = \\ &= e^{-\frac{i}{\hbar} \mathcal{H}_f t} \tilde{\mathbf{c}}. \end{aligned} \quad (\text{E11})$$

For clarity, we remark that in the first and second lines of Eq. (E11), the exponentialized operators are acting element-wise, on the Fock-space operators forming the vector $\tilde{\mathbf{c}}$. However, in the third line, the exponentialized operator is a 6×6 matrix acting on the 6-dimensional vector formed by $\tilde{\mathbf{c}}$.

Inserting Eq. (E11) into Eq. (E10) yields

$$\begin{aligned} P_{1 \leftarrow e}(t) &= \langle \Psi_e | \left[e^{-\frac{i}{\hbar} \mathcal{H}_f t} U_{\text{diag}}^\dagger \tilde{\mathbf{d}} \right]_6 \left[e^{-\frac{i}{\hbar} \mathcal{H}_f t} U_{\text{diag}}^\dagger \tilde{\mathbf{d}} \right]_3 | \Psi_e \rangle \\ &\equiv \sum_{m,n=1}^6 S_{mn}(t) \langle \Psi_e | \tilde{d}_m \tilde{d}_n | \Psi_e \rangle, \end{aligned} \quad (\text{E12})$$

where the second line is an implicit definition of the matrix

$$S_{mn}(t) = \left[e^{-\frac{i}{\hbar} \mathcal{H}_f t} U_{\text{diag}}^\dagger \right]_{6m} \left[e^{-\frac{i}{\hbar} \mathcal{H}_f t} U_{\text{diag}}^\dagger \right]_{3n}. \quad (\text{E13})$$

Following our notation introduced earlier, \tilde{d}_m denotes the m th component of the vector $\tilde{\mathbf{d}}$. Evaluating the matrix elements in Eq. (E12) yields

$$P_{1 \leftarrow e}(t) = \sum_{\mu=1}^3 S_{\mu, 3+\mu}(t). \quad (\text{E14})$$

This can be evaluated after the propagator and the BdG eigenvectors in Eq. (E13) have been obtained, e.g., numerically.

So far, we have assumed that our initial state is the even ground state $|\Psi_e\rangle$ of our initial Hamiltonian H_i . Depending on the values of the on-site energies ε_1 and ε_2 , the actual ground state of the wire can be either even or odd. For small on-site energy disorder $\sigma_{\text{noise}} \ll v = \Delta$, as considered in the main text, the lowest positive BdG quasiparticle excitation energy, say λ_1 , is much smaller than the other quasiparticle excitation energies. If the even ground state is the actual ground state, then the odd ground state is $|\Psi_o\rangle = d_1^\dagger |\Psi_e\rangle$. If the initial state is this odd ground state, then the time-dependent occupation probability of the dot reads

$$P_{1 \leftarrow o}(t) = \sum_{m,n=1}^6 S_{mn}(t) \langle \Psi_e | d_1 \tilde{d}_m \tilde{d}_n d_1^\dagger | \Psi_e \rangle. \quad (\text{E15})$$

By evaluating the matrix elements, we find

$$P_{1 \leftarrow o}(t) = S_{4,1}(t) + \sum_{\mu=2}^3 S_{\mu, 3+\mu}(t). \quad (\text{E16})$$

We have used the expressions (E13), (E14), (E16) to perform the numerical calculations leading to Fig. 7.

* palyi@mail.bme.hu

¹ A Yu Kitaev, "Unpaired Majorana fermions in quantum

wires," *Physics-Uspekhi* **44**, 131 (2001).

² Jason Alicea, Yuval Oreg, Gil Refael, Felix von Oppen,

- and Matthew P. A. Fisher, “Non-abelian statistics and topological quantum information processing in 1D wire networks,” *Nature Physics* **7**, 412 EP – (2011).
- ³ Martin Leijnse and Karsten Flensberg, “Introduction to topological superconductivity and Majorana fermions,” *Semiconductor Science and Technology* **27**, 124003 (2012).
 - ⁴ David Aasen, Michael Hell, Ryan V. Mishmash, Andrew Higginbotham, Jeroen Danon, Martin Leijnse, Thomas S. Jespersen, Joshua A. Folk, Charles M. Marcus, Karsten Flensberg, and Jason Alicea, “Milestones toward Majorana-based quantum computing,” *Phys. Rev. X* **6**, 031016 (2016).
 - ⁵ Chetan Nayak, Steven H. Simon, Ady Stern, Michael Freedman, and Sankar Das Sarma, “Non-abelian anyons and topological quantum computation,” *Rev. Mod. Phys.* **80**, 1083–1159 (2008).
 - ⁶ V. Mourik, K. Zuo, S. M. Frolov, S. R. Plissard, E. P. A. M. Bakkers, and L. P. Kouwenhoven, “Signatures of Majorana fermions in hybrid superconductor-semiconductor nanowire devices,” *Science* **336**, 1003–1007 (2012).
 - ⁷ S. M. Albrecht, A. P. Higginbotham, M. Madsen, F. Kuemmeth, T. S. Jespersen, J. Nygård, P. Krogstrup, and C. M. Marcus, “Exponential protection of zero modes in Majorana islands,” *Nature* **531**, 206 EP – (2016).
 - ⁸ J. Wiedenmann, E. Bocquillon, R. S. Deacon, S. Hartinger, O. Herrmann, T. M. Klapwijk, L. Maier, C. Ames, C. Brüne, C. Gould, A. Oiwa, K. Ishibashi, S. Tarucha, H. Buhmann, and L. W. Molenkamp, “4- π -periodic Josephson supercurrent in HgTe-based topological Josephson junctions,” *Nature Communications* **7**, 10303 EP – (2016).
 - ⁹ Leonid P. Rokhinson, Xinyu Liu, and Jacek K. Furdyna, “The fractional a.c. Josephson effect in a semiconductor–superconductor nanowire as a signature of Majorana particles,” *Nature Physics* **8**, 795 EP – (2012).
 - ¹⁰ Dominique Laroche, Danil Bouman, David J. van Woerkom, Alex Proutski, Chaitanya Murthy, Dmitry I. Pikulin, Chetan Nayak, Ruben J. J. van Gulik, Jesper Nygard, Peter Krogstrup, Leo P. Kouwenhoven, and Attila Geresdi, *ArXiv:1712.08459* (unpublished).
 - ¹¹ Stevan Nadj-Perge, Ilya K. Drozdov, Jian Li, Hua Chen, Sangjun Jeon, Jungpil Seo, Allan H. MacDonald, B. Andrei Bernevig, and Ali Yazdani, “Observation of Majorana fermions in ferromagnetic atomic chains on a superconductor,” *Science* (2014).
 - ¹² Howon Kim, Alexandra Palacio-Morales, Thore Posske, Levente Rózsa, Krisztián Palotás, László Szunyogh, Michael Thorwart, and Roland Wiesendanger, “Toward tailoring Majorana bound states in artificially constructed magnetic atom chains on elemental superconductors,” *Science Advances* **4** (2018).
 - ¹³ Rémy Pawlak, Marcin Kisiel, Jelena Klinovaja, Tobias Meier, Shigeki Kawai, Thilo Glatzel, Daniel Loss, and Ernst Meyer, “Probing atomic structure and Majorana wavefunctions in mono-atomic Fe chains on superconducting Pb surface,” *Npj Quantum Information* **2**, 16035 EP – (2016).
 - ¹⁴ Ramon Aguado, “Majorana quasiparticles in condensed matter,” *La Rivista del Nuovo Cimento* **40**, 523 (2017).
 - ¹⁵ Karsten Flensberg, “Non-abelian operations on Majorana fermions via single-charge control,” *Phys. Rev. Lett.* **106**, 090503 (2011).
 - ¹⁶ Kaveh Gharavi, Darryl Hoving, and Jonathan Baugh, “Readout of Majorana parity states using a quantum dot,” *Phys. Rev. B* **94**, 155417 (2016).
 - ¹⁷ Olesia Dmytruk, Mircea Trif, and Pascal Simon, “Cavity quantum electrodynamics with mesoscopic topological superconductors,” *Phys. Rev. B* **92**, 245432 (2015).
 - ¹⁸ Torsten Karzig, Christina Knapp, Roman M. Lutchyn, Parsa Bonderson, Matthew B. Hastings, Chetan Nayak, Jason Alicea, Karsten Flensberg, Stephan Plugge, Yuval Oreg, Charles M. Marcus, and Michael H. Freedman, “Scalable designs for quasiparticle-poisoning-protected topological quantum computation with Majorana zero modes,” *Phys. Rev. B* **95**, 235305 (2017).
 - ¹⁹ Arne L. Grimsmo and Thomas B. Smith, “Majorana qubit readout using longitudinal qubit-resonator interaction,” *Phys. Rev. B* **99**, 235420 (2019).
 - ²⁰ Stephan Plugge, Asbjørn Rasmussen, Reinhold Egger, and Karsten Flensberg, “Majorana box qubits,” *New Journal of Physics* **19**, 012001 (2017).
 - ²¹ Christina Knapp, Torsten Karzig, Roman M. Lutchyn, and Chetan Nayak, “Dephasing of Majorana-based qubits,” *Phys. Rev. B* **97**, 125404 (2018).
 - ²² Morten I. K. Munk, Reinhold Egger, and Karsten Flensberg, “Fidelity and visibility loss in Majorana qubits by entanglement with environmental modes,” *Phys. Rev. B* **99**, 155419 (2019).
 - ²³ T. Hyart, B. van Heck, I. C. Fulga, M. Burrello, A. R. Akhmerov, and C. W. J. Beenakker, “Flux-controlled quantum computation with Majorana fermions,” *Phys. Rev. B* **88**, 035121 (2013).
 - ²⁴ Parsa Bonderson, Michael Freedman, and Chetan Nayak, “Measurement-only topological quantum computation,” *Phys. Rev. Lett.* **101**, 010501 (2008).
 - ²⁵ A. R. Akhmerov, “Topological quantum computation away from the ground state using majorana fermions,” *Phys. Rev. B* **82**, 020509 (2010).
 - ²⁶ F Hassler, A R Akhmerov, and C W J Beenakker, “The top-transmon: a hybrid superconducting qubit for parity-protected quantum computation,” *New Journal of Physics* **13**, 095004 (2011).
 - ²⁷ Martin Leijnse and Karsten Flensberg, “Parity qubits and poor man’s Majorana bound states in double quantum dots,” *Phys. Rev. B* **86**, 134528 (2012).
 - ²⁸ Jay D. Sau and S. Das Sarma, “Realizing a robust practical Majorana chain in a quantum-dot-superconductor linear array,” *Nature Communications* **3**, 964 EP – (2012).
 - ²⁹ Ion C Fulga, Arbel Haim, Anton R Akhmerov, and Yuval Oreg, “Adaptive tuning of Majorana fermions in a quantum dot chain,” *New Journal of Physics* **15**, 045020 (2013).
 - ³⁰ Silas Hoffman, Constantin Schrade, Jelena Klinovaja, and Daniel Loss, “Universal quantum computation with hybrid spin-majorana qubits,” *Phys. Rev. B* **94**, 045316 (2016).
 - ³¹ Silas Hoffman, Denis Chevallier, Daniel Loss, and Jelena Klinovaja, “Spin-dependent coupling between quantum dots and topological quantum wires,” *Phys. Rev. B* **96**, 045440 (2017).
 - ³² Leon C. Camenzind, Liuqi Yu, Peter Stano, Jeremy D. Zimmerman, Arthur C. Gossard, Daniel Loss, and Dominik M. Zumbühl, “Hyperfine-phonon spin relaxation in a single-electron GaAs quantum dot,” *Nature Communications* **9**, 3454 (2018).
 - ³³ Davyd Razmadze, Deividas Sabonis, Filip K. Malinowski, Gerbold C. Ménard, Sebastian Pauka, Hung Nguyen, David M.T. van Zanten, Eoin C.T. O’Farrell, Judith Suter, Peter Krogstrup, Ferdinand Kuemmeth, and Charles M. Marcus, “Radio-frequency methods for

- Majorana-based quantum devices: Fast charge sensing and phase-diagram mapping,” *Phys. Rev. Applied* **11**, 064011 (2019).
- ³⁴ M. A. Nielsen and I. L. Chuang, *Quantum Computation and Quantum Information* (Cambridge University Press, 2000).
- ³⁵ Frank et al. Arute, “Quantum supremacy using a programmable superconducting processor,” *Nature* **574**, 505–510 (2019).
- ³⁶ Robert Raussendorf and Hans J. Briegel, “A one-way quantum computer,” *Phys. Rev. Lett.* **86**, 5188–5191 (2001).
- ³⁷ J. F. Steiner and F. von Oppen, “Readout of Majorana qubits,” *ArXiv:2004.02124* (unpublished).
- ³⁸ M. I. K. Munk, J. Schulenburg, R. Egger, and K. Flensberg, “Parity-to-charge conversion in Majorana qubit readout,” *ArXiv:2004.02123* (unpublished).
- ³⁹ T. Hayashi, T. Fujisawa, H. D. Cheong, Y. H. Jeong, and Y. Hirayama, “Coherent manipulation of electronic states in a double quantum dot,” *Phys. Rev. Lett.* **91**, 226804 (2003).
- ⁴⁰ K. D. Petersson, J. R. Petta, H. Lu, and A. C. Gosard, “Quantum coherence in a one-electron semiconductor charge qubit,” *Phys. Rev. Lett.* **105**, 246804 (2010).
- ⁴¹ Zhan Shi, C. B. Simmons, Daniel R. Ward, J. R. Prance, R. T. Mohr, Teck Seng Koh, John King Gamble, Xian Wu, D. E. Savage, M. G. Lagally, Mark Friesen, S. N. Coppersmith, and M. A. Eriksson, “Coherent quantum oscillations and echo measurements of a Si charge qubit,” *Phys. Rev. B* **88**, 075416 (2013).
- ⁴² Blake M. Freeman, Joshua S. Schoenfeld, and HongWen Jiang, “Comparison of low frequency charge noise in identically patterned Si/SiO₂ and Si/SiGe quantum dots,” *Applied Physics Letters* **108**, 253108 (2016).
- ⁴³ L. Petit, J. M. Boter, H. G. J. Eenink, G. Droulers, M. L. V. Tagliaferri, R. Li, D. P. Franke, K. J. Singh, J. S. Clarke, R. N. Schouten, V. V. Dobrovitski, L. M. K. Vandersypen, and M. Veldhorst, “Spin lifetime and charge noise in hot silicon quantum dot qubits,” *Phys. Rev. Lett.* **121**, 076801 (2018).
- ⁴⁴ Jun Yoneda, Kenta Takeda, Tomohiro Otsuka, Takashi Nakajima, Matthieu R. Delbecq, Giles Allison, Takumu Honda, Tetsuo Kodera, Shunri Oda, Yusuke Hoshi, Noritaka Usami, Kohei M. Itoh, and Seigo Tarucha, “A quantum-dot spin qubit with coherence limited by charge noise and fidelity higher than 99.9%,” *Nature Nanotechnology* **13**, 102–106 (2018).
- ⁴⁵ Xin Wang, Lev S. Bishop, J. P. Kestner, Edwin Barnes, Kai Sun, and S. Das Sarma, “Composite pulses for robust universal control of singlet–triplet qubits,” *Nature Communications* **3**, 997 (2012).
- ⁴⁶ Guilherme Tosi, Fahd A. Mohiyaddin, Vivien Schmitt, Stefanie Tenberg, Rajib Rahman, Gerhard Klimeck, and Andrea Morello, “Silicon quantum processor with robust long-distance qubit couplings,” *Nature Communications* **8**, 450 (2017).
- ⁴⁷ T. F. Watson et al., “A programmable two-qubit quantum processor in silicon,” *Nature* **555**, 633 (2018).
- ⁴⁸ Jelmer M. Boter, Xiao Xue, Tobias S. Krahenmann, Thomas F. Watson, Vickram N. Premakumar, Daniel R. Ward, Donald E. Savage, Max G. Lagally, Mark Friesen, Susan N. Coppersmith, Mark A. Eriksson, Robert Joynt, and Lieven M. K. Vandersypen, *ArXiv:1906.02731* (unpublished).
- ⁴⁹ P. Krogstrup, N. L. B. Ziino, W. Chang, S. M. Albrecht, M. H. Madsen, E. Johnson, J. Nygård, C. ? M. Marcus, and T. S. Jespersen, “Epitaxy of semiconductor-superconductor nanowires,” *Nature Materials* **14**, 400 EP – (2015), article.
- ⁵⁰ R. M. Lutchyn, E. P. A. M. Bakkers, L. P. Kouwenhoven, P. Krogstrup, C. M. Marcus, and Y. Oreg, “Majorana zero modes in superconductor-semiconductor heterostructures,” *Nature Reviews Materials* **3**, 52–68 (2018).
- ⁵¹ J. Shabani, M. Kjaergaard, H. J. Suominen, Younghyun Kim, F. Nichele, K. Pakrouski, T. Stankevic, R. M. Lutchyn, P. Krogstrup, R. Feidenhans’l, S. Kraemer, C. Nayak, M. Troyer, C. M. Marcus, and C. J. Palmstrøm, “Two-dimensional epitaxial superconductor-semiconductor heterostructures: A platform for topological superconducting networks,” *Phys. Rev. B* **93**, 155402 (2016).
- ⁵² H. J. Suominen, M. Kjaergaard, A. R. Hamilton, J. Shabani, C. J. Palmstrøm, C. M. Marcus, and F. Nichele, “Zero-energy modes from coalescing Andreev states in a two-dimensional semiconductor-superconductor hybrid platform,” *Phys. Rev. Lett.* **119**, 176805 (2017).
- ⁵³ Fabrizio Nichele, Asbjørn C. C. Drachmann, Alexander M. Whicar, Eoin C. T. O’Farrell, Henri J. Suominen, Antonio Fornieri, Tian Wang, Geoffrey C. Gardner, Candice Thomas, Anthony T. Hatke, Peter Krogstrup, Michael J. Manfra, Karsten Flensberg, and Charles M. Marcus, “Scaling of Majorana zero-bias conductance peaks,” *Phys. Rev. Lett.* **119**, 136803 (2017).
- ⁵⁴ Yuriy Makhlin, Gerd Schön, and Alexander Shnirman, “Dissipation in Josephson qubits,” in *New Directions in Mesoscopic Physics (Towards Nanoscience)*, edited by R. Fazio, V. F. Gantmakher, and Y. Imry (Springer Netherlands, Dordrecht, 2003) pp. 197–224.
- ⁵⁵ Alexander V. Khaetskii and Yuli V. Nazarov, “Spin-flip transitions between Zeeman sublevels in semiconductor quantum dots,” *Phys. Rev. B* **64**, 125316 (2001).
- ⁵⁶ P. Y. Yu and M. Cardona, *Fundamentals of Semiconductors* (Springer, 2010).
- ⁵⁷ Roman M. Lutchyn, Jay D. Sau, and S. Das Sarma, “Majorana fermions and a topological phase transition in semiconductor-superconductor heterostructures,” *Phys. Rev. Lett.* **105**, 077001 (2010).
- ⁵⁸ Yuval Oreg, Gil Refael, and Felix von Oppen, “Helical liquids and Majorana bound states in quantum wires,” *Phys. Rev. Lett.* **105**, 177002 (2010).
- ⁵⁹ Péter Boross, János K. Asbóth, Gábor Széchenyi, László Oroszlány, and András Pályi, “Poor man’s topological quantum gate based on the su-schrieffer-heeger model,” *Phys. Rev. B* **100**, 045414 (2019).
- ⁶⁰ Christina Knapp, Michael Zaletel, Dong E. Liu, Meng Cheng, Parsa Bonderson, and Chetan Nayak, “The nature and correction of diabatic errors in anyon braiding,” *Phys. Rev. X* **6**, 041003 (2016).
- ⁶¹ Chia-Hsien Huang, Chih-Hwan Yang, Chien-Chang Chen, Andrew S. Dzurak, and Hsi-Sheng Goan, “High-fidelity and robust two-qubit gates for quantum-dot spin qubits in silicon,” *Phys. Rev. A* **99**, 042310 (2019).
- ⁶² J. A. Krzywda and L. Cywinski, “Adiabatic electron charge transfer between two quantum dots in presence of $1/f$ noise,” *Phys. Rev. B* **101**, 035303 (2020).
- ⁶³ R. V. Mishmash, B. Bauer, F. von Oppen, and J. Alicea, “Dephasing and leakage dynamics of noisy Majorana-based qubits: Topological versus Andreev,” *ArXiv:1911.02582*

- (unpublished).
- ⁶⁴ J. M. Elzerman, R. Hanson, L. H. Willems van Beveren, B. Witkamp, L. M. K. Vandersypen, and L. P. Kouwenhoven, “Single-shot read-out of an individual electron spin in a quantum dot,” *Nature* **430**, 431–435 (2004).
 - ⁶⁵ R. Hanson, L. P. Kouwenhoven, J. R. Petta, S. Tarucha, and L. M. K. Vandersypen, “Spins in few-electron quantum dots,” *Rev. Mod. Phys.* **79**, 1217–1265 (2007).
 - ⁶⁶ Lajos Diisi, *A Short Course in Quantum Information Theory: An Approach From Theoretical Physics* (Springer-Verlag Berlin Heidelberg, 2007).
 - ⁶⁷ M. S. Scheurer and A. Shnirman, “Nonadiabatic processes in Majorana qubit systems,” *Phys. Rev. B* **88**, 064515 (2013).